Journal of Mathematical Biology (2026) 92:75
https://doi.org/10.1007/s00285-026-02390-6

Mathematical Biology

Theory and simulations of delayed stochastic and deterministic models of prion diseases

Gangadhara Boregowda[1] · Omar Sharif[1] · Daniel Gutierrez III[1] · Allegra Simmons[2] · Laurent Pujo-Menjouet[3] · Tamer Oraby[1] · Michael R. Lindstrom[1]

Received: 18 August 2025 / Revised: 5 February 2026 / Accepted: 25 March 2026
© The Author(s) 2026

Abstract
Neurodegenerative diseases (NDs), such as Alzheimer's, Parkinson's, and prion diseases, are characterized by the dynamical spread of toxic proteins through the brain. In prion diseases, cellular prion protein (PrP^{C}), produced by neurons, misfolds into a toxic form, known as scrapie prion protein (PrP^{Sc}). PrP^{Sc} induces neuronal stress which ultimately leads to cell death. In this paper, we develop mathematical models for the progression of prion diseases, incorporating a cellular defense mechanism that introduces a delay term affecting protein translation and a volatility term accounting for unaccounted biological factors influencing the system. We also extend the model to capture the spatial spread of toxic proteins over the brain connectome. Our first objective is to establish the existence and uniqueness of a global positive solution to the prion disease models. Afterwards, we analyze the asymptotic behavior of the models by identifying regimes of persistence and extinction of toxic proteins. For the deterministic delayed systems, we perform a stability analysis for the persistence and demonstrate that the system undergoes a Hopf bifurcation. We also study the intensity of fluctuations of the equilibrium state of the stochastic model. Additionally, we present numerical simulations to illustrate the model dynamics using biologically relevant parameters.

Keywords Prion disease · Unfolded Protein Response · Delayed stochastic differential equation · Global existence-uniqueness · Extinction-persistence · Hopf bifurcation

✉ Gangadhara Boregowda
gangadhara.boregowda@utrgv.edu

[1] School of Mathematical and Statistical Sciences, The University of Texas Rio Grande Valley, Edinburg, Texas, USA

[2] Department of Mathematics, The University of Dallas, Irving, Texas, USA

[3] Department of Mathematics, Universite Claude Bernard Lyon 1, CNRS, Centrale de Lyon, INSA Lyon, Université Jean Monnet, ICJ UMR5208, Inria, 69622 Villeurbanne, France

Published online: 23 April 2026

Mathematics Subject Classification 60H10 · 60H30 · 93D05

1 Introduction

Neurodegenerative diseases (NDs) are serious disorders that gradually damage the brain and central nervous tissue, causing cognitive decline, behavioral and neurological changes, and eventually, death. The most common NDs diseases are Alzheimer's disease (AD) (Goedert and Spillantini 2006) and Parkinson's disease (PD) (Davie 2008), while prion diseases (Geschwind 2015) are comparatively rare. Despite differences in symptoms, progression, and affected brain regions, many NDs share common features. A key similarity is the accumulation of toxic proteins spreading through the brain (Shaheen et al. 2023; Fornari et al. 2019), which are believed to impair neuronal function or cause cell death (Kiaei 2013). Postmortem examination of brain tissues of affected individuals confirms the presence of toxic proteins (Akhtar et al. 2021). For instance, in AD, both the accumulation of Amyloid-beta plaques outside cells and tau protein tangles inside cells are commonly detected and are believed to drive the progression of the disease (Jack et al. 2018; Ono et al. 2009; Tolar et al. 2020). In PD, Alpha-synuclein is thought to be the primary pathogenic protein (Stefanis 2012); and in prion diseases, it is scrapie protein (Genereux and Wiseman 2015; Prusiner 1989).

Cellular prion protein (PrP^C) is naturally produced by neurons. Scrapie prion protein (PrP^{Sc}) is a misfolded version of PrP^C which is protease-resistant and toxic (DebBurman et al. 1997). During the spread of prion diseases, PrP^{Sc} interacts with PrP^C inducing a conformational change in PrP^C turning it into PrP^{Sc}.

This process leads to the accumulation of misfolded prions, resulting in neuronal dysfunction and cell death (Atkinson et al. 2016; Selkoe 2003). The high concentrations of PrP^{Sc} in the close vicinity of the cell triggers the Unfolded Protein Response (UPR), leading to a temporary reduction or complete halt in its protein synthesis, thereby decreasing the production of healthy proteins (Moreno et al. 2012). This adaptive response helps to limit the accumulation of PrP^{Sc} and facilitates the natural clearance of toxic proteins by diffusion and degradation, ultimately allowing neurons to resume their normal cellular functions. The UPR activation results in an upregulation of endoplasmic reticulum (ER) kinases, which suppress protein translation to alleviate stress (Moreno et al. 2012, 2013). However, prolonged or excessive activation of the UPR can initiate a cascade of events leading to apoptotic cell death (Livezey et al. 2018).

In recent years, mathematical models have significantly advanced our understanding of neurodegenerative diseases (NDs). From a modeling perspective, three main approaches have been developed to describe ND dynamics. The first comprises kinetic growth and fragmentation models, which employ systems of ordinary differential equations (ODEs) to capture local interactions among protein aggregates of different sizes (Fornari et al. 2019; Assembly 2002). The second approach, known as network diffusion or connectome-based models, uses dynamical processes on brain networks to investigate the global prion-like propagation of misfolded proteins along structural connectivity pathways (Raj et al. 2012; Tora et al. 2025). The third approach consists of reaction–diffusion-based continuum models formulated as partial differential

equations (PDEs), which describe the spatiotemporal evolution of toxic proteins in the brain and their interaction with tissue properties (Weickenmeier et al. 2019; Bertsch et al. 2017; Miller et al. 2024).

These mathematical frameworks have been applied to study a broad range of neurodegenerative disorders and mechanisms, including Alzheimer's disease (AD) (Hao and Friedman 2016; Lindstrom et al. 2021; Bertsch et al. 2023), Parkinson's disease (PD) (Desplats et al. 2009), and cellular stress responses such as the unfolded protein response (UPR) (Adimy et al. 2022; Miller et al. 2024). In particular, connectome-informed PDE and network models have demonstrated that the spatial spreading of toxic proteins is strongly influenced by brain connectivity, regional heterogeneity, and transport mechanisms, providing critical insights into disease progression over time (Fornari et al. 2019; Shaheen et al. 2023; Tora et al. 2025; Fornari et al. 2020).

In biological systems, both delays and random noise are inherent to various processes. The deterministic models can be extended to stochastic models by introducing an additional source of variability known as system noise. This system noise, which may represent a continuous stochastic process, is incorporated into the differential equations to account for random fluctuations in the evolution of the system states (Saqlain et al. 2020). Time delay has been introduced to model the UPR in prion diseases (Adimy et al. 2022; Miller et al. 2024). Literature suggests (Adimy et al. 2022; Miller et al. 2024; Boregowda and Lindstrom 2025) that the time delay may induce a Hopf bifurcation in the concentration of toxic proteins, where oscillations can be turned on or off depending on the parameter regimes.

A major challenge in SDE, ODE, and PDE-based modeling lies in establishing the existence, uniqueness, and stability of their solutions. In practice, especially in engineering, models are often analyzed numerically under the assumption that a solution exists within a defined solution space (Chung 2002; Miller et al. 2024). Existence theory for SDEs and PDEs is well studied in the literature. For instance, in the case of SDE-based models, see (Mao 2007) and for PDE-based models, see (Pao 2012). Moreover, in disease modeling, it is important to understand the long-term dynamics of the solution to predict the behavior of the disease.

In this paper, we present a mathematical model that incorporates various special case models for the dynamics and spread of prion diseases. We incorporate stochasticity and the UPR mechanism into the model to more accurately capture prion dynamics in a biologically realistic manner. The spatial spreading of toxic proteins in the brain is modeled using the brain connectome, leading to a system of DEs or SDEs. This work begins by establishing the existence of unique, global, positive solutions to the new models. Furthermore, we derive conditions on nondimensional parameters to predict the dynamics of our model, such as the persistence and extinction of toxic proteins. We also show that the presence of a time delay can induce oscillations in the levels of toxic proteins under certain parameter regimes. Additionally, we demonstrate that the stochastic solution converges to the positive equilibrium point of the deterministic solution for small noise. We validate our theoretical findings through numerical simulations using synthetic data. Finally, we present the spatial spread of toxic proteins using the human brain connectome.

The structure of the paper is as follows: Section 2 presents the derivation of the mathematical model and provides biological insights into prion diseases. Section 3

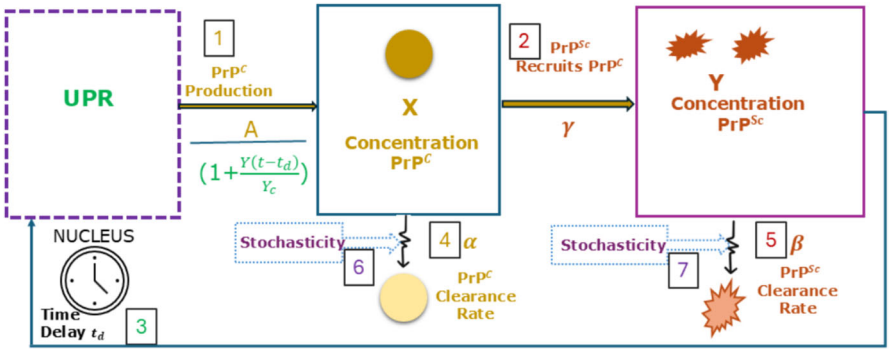

Fig. 1 Schematic illustration of the protein misfolding process

covers the results of this paper. The existence and uniqueness theory for the models is discussed in subsection 3.1. In subsection 3.2, we derive the conditions governing the persistence and extinction of toxic proteins. Subsection 3.3 presents the asymptotic analysis of the mathematical model, including the Hopf bifurcation. We validate the theoretical findings with numerical simulation results in Section 4, specifically using simulations with clinical data presented in Section 4.5, followed by a discussion of the biological implications in Section 5. Finally, Section 6 presents the conclusion and limitations of the work. Additional supporting definitions and results are included in the Appendix.

2 Mathematical model of the prion growth

In this section, we focus on understanding the biology of prion diseases and derive a mathematical model describing prion spread through the brain.

Fig. 1 represents the biological mechanisms in a mathematical framework evolving over time t. With process 1, PrP^C is produced at a rate $\leq A$ (depending on the UPR — see later) resulting in an accumulation of PrP^C (dark yellow circles) with concentration X. In process 2, PrP^{Sc} (red spiky shapes) with concentration Y recruits PrP^C at a rate γ to misfold into PrP^{Sc}. The concentration of PrP^{Sc} governs the UPR stress response (process 3) which, after a biological delay t_d, modifies the resulting production rate of PrP^c. For simplicity, we model this effect using a multiplicative factor of form $\left(1+\frac{Y(t-t_d)}{Y_c}\right)^{-1}$, rather than the more general expression $\left(1+(\frac{Y(t-t_d)}{Y_c})^m\right)^{-1}$, $m>0$. Both PrP^C and PrP^{Sc} are subject to clearance at respective rates α (process 4) and β (process 5). Stochasticity, processes 6 and 7, affects both clearances.

2.1 Single region model overview

We unveil the spatiotemporal dynamics of the UPR using a simplified model. We let $X(t)$ be the concentration of PrP^C at time t and $Y(t)$ be the concentration of PrP^{Sc}

at time t. The model captures the misfolding of PrP^C into PrP^{Sc} upon interaction with PrP^{Sc}. We do not consider higher-order structures, such as dimers, oligomers, nuclei, or fibrils. This mechanism is commonly known as the heterodimer model. Since PrP^{Sc} downregulates the production of PrP^C, we model this negative feedback using a decreasing Hill function (with delay). To account for fluctuations in the clearance of PrP^C and PrP^{Sc} due to temporal heterogeneities in the brain's capacity to clear proteins, we assume there are stochastic fluctuations in the clearance rate of PrP^{Sc}. For simplicity, we do not model noise on the recruitment or production processes. Under these assumptions, the model is described by the following system:

$$\begin{aligned} \mathrm{d}X &= \left(\frac{A}{1 + \frac{Y(t-t_d)}{Y_c}} - \gamma XY - \alpha X \right) \mathrm{d}t + \rho_X X \mathrm{d}W_X(t), \\ X(0) &= \hat{X}, \end{aligned} \tag{1}$$

$$\begin{aligned} \mathrm{d}Y &= (\gamma XY - \beta Y)\mathrm{d}t + \rho_Y Y \mathrm{d}W_Y(t), \\ Y(0) &= \hat{Y}(t), -t_d \leq t \leq 0, \end{aligned} \tag{2}$$

where $A > 0$ represents the maximum production rate of PrP^C; $Y_c > 0$ is a sensitivity threshold for PrP^{Sc}; $\gamma \geq 0$ is the conversion rate of PrP^C to PrP^{Sc}; $\alpha \geq 0$ is the clearance rate of PrP^C; $\beta \geq 0$ is the clearance rate of PrP^{Sc}; the terms $\rho_X X \mathrm{d}W_X(t)$ and $\rho_Y Y \mathrm{d}W_Y(t)$ with $\rho_X, \rho_Y \geq 0$ model fluctuations in PrP^C and PrP^{Sc} clearance, respectively, with stochastic Wiener processes (Saqlain et al. 2020; Ditlevsen and Samson 2012); $Y(t - t_d)$ is the concentration of the toxic protein at a time $t_d \geq 0$ in the past; $\hat{X}$ is the initial concentration of PrP^C; and $\hat{Y}$ is an initial concentration history for PrP^{Sc}.

Because PrP^{Sc} formation relies on the availability of PrP^C, UPR activation indirectly slows PrP^{Sc} propagation by limiting substrate supply. Activation of the UPR is not instantaneous; cells require time to detect misfolded proteins, initiate signaling cascades, and adjust their protein synthesis and degradation machinery (Peña and Harris 2011). To capture this latency, we model protein synthesis at time t as a function of the system's state at an earlier time $t - t_d$, where $t_d \geq 0$ represents the total duration of UPR-associated processes leading to global translation attenuation.

We use a white noise to model intrinsic, small, continuous fluctuations in the clearance rate of prions rather than rare catastrophic events induced by other types of noise like Lévy noise (Applebaum 2009). Through dimensional analysis (see Appendix F), we choose to model $\rho_X = \sigma\sqrt{\alpha}$ and $\rho_Y = \sigma\sqrt{\beta}$ for a dimensionless $O(1)$ constant $\sigma \geq 0$. The physical dimensions and definitions are described in Table 1.

The slow clearance rate of the pathogenic PrP^{Sc} protein relative to the healthy PrP^C protein is a chief characteristic of prion diseases. By defining $0 < \epsilon := \frac{\beta}{\alpha} \ll 1$ as an asymptotic scale, the appropriate leading order system (see Appendix E) for PrP^{Sc} is

Table 1 Model parameters and global notations with descriptions and physical dimensions (M = mass, L = length, T = time)

Parameter	Description	Dimension
A	Production rate of PrP^C	$M/(L^3\,T)$
γ	Rate of recruitment of PrP^C into the misfolded state through interaction with PrP^{Sc}	$L^3/(M\,T)$
Y	Concentration of PrP^{Sc}	M/L^3
X	Concentration of PrP^C	M/L^3
Y_c	UPR-triggering concentration of PrP^{Sc}	M/L^3
α	Clearance rate of PrP^C	$1/T$
β	Clearance rate of PrP^{Sc}	$1/T$
t_d	Time delay	T
ρ_X	PrP^C clearance noise intensity	$1/T^{\frac{1}{2}}$
ρ_Y	PrP^{Sc} clearance noise intensity	$1/T^{\frac{1}{2}}$
σ	Dimensionless noise to square root of clearance rate ratio	1
σ_i	Dimensionless noise to square root of clearance rate ratio in region i	1
$L_{i,j}$	Edge weight between node j and i	1/L
r	Overall fitted constant	L/T

$$\begin{aligned} dY &= \left(\frac{\gamma A Y}{\left(1 + \frac{Y(t-t_d)}{Y_c}\right)(\gamma Y + \alpha)} - \beta Y \right) dt + \sigma \sqrt{\beta} Y dW(t), \quad t \geq 0 \\ Y(t) &= \hat{Y}(t), \quad -t_d \leq t \leq 0. \end{aligned} \tag{3}$$

Formally speaking, (1) equilibrates rapidly (in distribution) and (2) only works with the average equilibrated X.

To nondimensionalize and rescale equation (3), we apply the transformations $t = \overline{t}\, t^*$ and $Y(t) = \overline{Y}\, U(t^*)$, where overbars denote dimensional scales and asterisks denote dimensionless variables. By substituting $\overline{t} = \frac{1}{\beta}$ and $\overline{Y} = \frac{A}{\beta}$, simplifying, and omitting the asterisks and overbars for convenience, we obtain (see Appendix E)

$$\begin{aligned} dU &= \left(\frac{U}{(1 + \eta U(t-\tau))(U + \zeta)} - U \right) dt + \sigma U dW(t), \quad t \geq 0 \\ U(t) &= \phi(t), \quad t \in [-\tau, 0], \end{aligned} \tag{4}$$

where

$$\eta = \frac{\overline{Y}}{Y_c}, \quad \zeta = \frac{\alpha\beta}{\gamma A}, \text{ and } \quad \tau = t_d \beta. \tag{5}$$

Here, U is the dimensionless toxic protein concentration ,$\overline{Y}$ is the characteristic scale of PrP^{Sc}, $\overline{t}$ is the characteristic time for PrP^{Sc} to be cleared, η represents the characteristic scale of PrP^{Sc} relative to its UPR-triggering concentration Y_c. The clinical values of

these parameters are listed in Table 8 (see Appendix F). The dimesionless parameter $\zeta = \frac{1}{R_0}$ where $R_0 = \frac{\gamma A}{\alpha\beta}$ is the average number of PrP^{Sc} generated from a single PrP^{Sc} in a protein population of PrP^{C}. This can be reasoned as follows: $\frac{A}{\alpha}$ is the steady state PrP^{C} concentration in the absence of scrapie; $\frac{1}{\beta}$ is the average lifespan of a PrP^{Sc} protein; thus, with recruitment rate γ, $\frac{A}{\alpha} \times \frac{1}{\beta} \times \gamma$ is the average number of scrapie proteins a single scrapie protein can recruit in its lifetime in a susceptible prion population. The behavior of the system depends critically on the value of the dimensionless parameters ζ and η.

2.2 Connectome model overview

Assuming that transport occurs only along axonal pathways, we represent the brain connectivity using the graph Laplacian constructed from the structural connectome (see, for example, (Fornari et al. 2020; Shaheen et al. 2023)). Such graph-based formulations are considered accurate and computationally efficient approximations of the corresponding continuous models, particularly in the context of heterodimer-type prion models (Fornari et al. 2019). To capture axonal transport, we represent the propagation of toxic proteins as a diffusion-like process on the structural brain connectome. The brain connectome is modeled as a weighted graph $\mathcal{G}$ with N nodes and E edges, where each node corresponds to a distinct region of the brain, and each edge represents a structural connection between two regions. These pathways provide biologically realistic routes for the spread of misfolded prion-like proteins. The connectivity of $\mathcal{G}$ is encoded in a weighted adjacency matrix $A_{i,j}$, where each entry is computed as the ratio of the mean fiber number $n_{i,j}$ to the fiber length $l_{i,j}$ between regions i and j. From the weighted adjacency matrix, we compute the weighted degree for each node i, and the edge weight between node i and j as

$$L_{i,j} = A_{i,j} \text{ with } A_{i,j} = \frac{n_{i,j}}{l_{i,j}} \text{ for } i \neq j,\ i, j = 1, 2, \ldots, N,$$
$$L_{i,i} = \sum_{j=1, j\neq i}^{N} A_{i,j}.$$

Let $X_i(t)$ and $Y_i(t)$ be the concentration of PrP^{C} and PrP^{Sc}, respectively at time t and region i. We note that the cellular prion protein exists in both membrane-bound and extracellular forms (Shafiq et al. 2022; Rangel et al. 2013). In this study, we assume that PrP^{C} is exclusively membrane-bound. This assumption restricts the transport of PrP^{C} between brain regions. We allow PrP^{Sc} to be transported between regions. Under these assumptions, the connectome-based model is described by the following system:

$$\begin{aligned} \mathrm{d}X_i &= \left(\frac{A}{1 + \frac{Y_i(t-t_d)}{Y_c}} - \gamma X_i Y_i - \alpha X_i \right) \mathrm{d}t + \rho_{X,i} X_i \mathrm{d}W_{X,i}(t), \\ X_i(0) &= \hat{X}_i, \end{aligned} \tag{6}$$

Table 2 List of modeling approaches for prion disease progression

Model type	Scalar model (equation (4))	System model (equation (8))
Deterministic Model	M: $\tau = 0, \sigma = 0$	MS: $\tau = 0, \sigma_i = 0$ for $i = 1, 2, \ldots, N$ when $N > 1$
Delay Deterministic Model	DM: $\tau > 0, \sigma = 0$	DMS: $\tau > 0, \sigma_i = 0$ for $i = 1, 2, \ldots, N$ when $N > 1$
Stochastic Differential Model	SM: $\tau = 0, \sigma > 0$	SMS: $\tau = 0, \sigma_i > 0$ for $i = 1, 2, \ldots, N$ when $N > 1$
Stochastic Delay Differential Model	SDM: $\tau > 0, \sigma > 0$	SDMS: $\tau > 0, \sigma_i > 0$ for $i = 1, 2, \ldots, N$ when $N > 1$

$$\begin{aligned} \mathrm{d}Y_i &= \left(r \sum_{j=1, j\neq i}^{N} L_{i,j} Y_j - r L_{i,i} Y_i + \gamma X_i Y_i - \beta Y_i \right) \mathrm{d}t + \rho_{Y,i} Y_i \mathrm{d}W_{Y,i}(t), \\ Y_i(t) &= \hat{Y}_i(t), \ t \in [-\tau, 0], \end{aligned} \tag{7}$$

for $i = 1, 2, \ldots, N$. The terms $\rho_{X,i} X_i \mathrm{d}W_{X,i}(t)$ and $\rho_{Y,i} Y_i \mathrm{d}W_{Y,i}(t)$ with $\rho_{X,i}, \rho_{Y,i} \geq 0$ model fluctuations in $\mathrm{PrP^C}$ and $\mathrm{PrP^{Sc}}$ clearance, respectively with stochastic Wiener processes at region i, $L_{i,j}$ represents the connectivity weight (edge weight) between regions j and i, and r is an overall fitted parameter with the dimension of velocity (see Appendix F). Further details of the brain network and the associated connectivity matrix are provided in Section 4.5. Similar to the single region case, we choose to model $\rho_{X,i} = \sigma_i \sqrt{\alpha}$ and $\rho_{Y,i} = \sigma_i \sqrt{\beta}$ for dimensionless $O(1)$ constants $\sigma_i \geq 0$, $i = 1, \ldots, N$.

Using the same arguments as in the scalar model (Section 2.1), we obtain the nondimensional model for the toxic concentration as below (see Appendix E for the derivation):

$$\begin{aligned} \mathrm{d}U_i(t) &= \left[\frac{U_i(t)}{(1 + \eta U_i(t-\tau))(U_i(t) + \zeta)} - U_i(t) - \omega_{i,i} U_i(t) \right. \\ &\qquad \left. + \sum_{j=1, j\neq i}^{N} \omega_{i,j} U_j(t) \right] \mathrm{d}t + \sigma_i U_i(t) \, \mathrm{d}W_i(t), \quad t \geq 0, \\ U_i(t) &= \phi_i(t), \quad t \in [-\tau, 0], \end{aligned} \tag{8}$$

for $i = 1, 2, \ldots, N$. Here $U_i(t)$ is the dimensionless toxic protein concentration in region i and $\omega_{i,j} = r \frac{L_{i,j}}{\beta}$ represents the dimensionless connectivity weight between regions j and i.

Equations (4) and (8) describe various biological phenomena. For analytical purposes, we consider specific cases of these equations and establish relevant theoretical results. In the subsequent sections, we refer to the models using abbreviated names, which are provided in Table 2.

Model assumptions

The underlying assumptions of the model are grounded in observed biological phenomena. Some studies construct symmetric connectivity matrices (Shaheen et al. 2023; Fornari et al. 2020), where symmetry typically arises from methodological choices and preprocessing steps used to derive matrices from empirical brain data. Non-symmetric connectivity matrices have also been reported (Škoch et al. 2022). Motivated by these observations, we develop a mathematical framework for a general connectome matrix that does not assume symmetry. Based on this framework, we propose the following assumptions, which form the foundation for deriving conditions on the parameters governing the dynamics of protein concentration.

Let $(\Omega, \mathcal{F}, P)$ be a complete probability space with a filtration $\{\mathcal{F}_t\}_{t\geq 0}$ that is increasing and right-continuous, while $\mathcal{F}_0$ contains all P-null sets. Let $W(t)$ and $W_i(t)$ be Brownian motions (or Wiener processes) defined on this probability space for $i = 1, 2, 3, \ldots, N$.

Assumptions

A1. $U_i(0) > 0$ for $i = 1, 2, \ldots, N$.
A2. $\phi_i(t) > 0$, $\phi_i \in \mathcal{C}([-\tau, 0], \mathbb{R}_+)$ for $i = 1, 2, \ldots, N$.
A3. $\tau, \zeta, \eta, \sigma_i \geq 0$, for $i = 1, 2, ..., N$.
A4. The elements of the connectivity matrix are $\omega_{i,j} \geq 0$, and $\omega_{i,i} = \sum_{j=1, j\neq i}^{N} \omega_{j,i}$, for $i, j = 1, 2, \ldots, N$.

3 Results

The key results of this study and their respective contributions are summarized in Table 3.

3.1 Existence and uniqueness

A primary concern in analyzing the long-term dynamical behavior of the model is the global existence of solutions. Additionally, for population dynamics models, it is crucial to ensure that the solutions remain nonnegative. Therefore, in this section, we establish the existence of global positive solutions for both the scalar and system stochastic delay differential equations. The existence theory for deterministic and delayed deterministic models follows directly from the theorems presented below. The analytical solution to M model is presented in Appendix D.

Theorem 1 *For any given initial value $U(0) \in \mathbb{R}_+$, there is a unique positive solution $U(t)$ to the SM model for $t \geq 0$ such that $U(t) \in \mathbb{R}_+$ for all $t \geq 0$ a.s.*

Table 3 Main results and contributions of this paper

Result	Contribution
Theorem 1, Corollary 2, and Remark 1	Establish existence of global positive solution of the M, DM, SM, and SDM
Theorem 3, Corollary 4, and Remark 2	Establish existence of global positive solution of the MS, DMS, SMS, and SDMS
Theorem 5	Derive the conditions of extinction and persistence of the toxic protein concentration in the SM
Theorem 6	Derive the conditions of extinction and weak persistence of the toxic protein concentration in the SMS
Theorem 8	Establish the asymptotic behavior of the SDM around the positive fixed point of DM
Theorem 10	Explore the stability and Hopf bifurcation for DM

Proof Let $r_0 = -\frac{1}{2}\min\left\{\frac{1}{\eta}, \zeta\right\}$. The function $g(t, U) = \sigma U$ satisfies the global Lipchitz and growth conditions in Theorem 3.1 (Mao 2007, p.51). However,

$$f(t, U) = \frac{U}{(1 + \eta U)(\zeta + U)} - U$$

has the singularity at $U = \frac{-1}{\eta}$ and $U = -\zeta$. Clearly, f satisfies the Lipchitz and growth conditions if $r_0 \leq U$. Therefore, we define the modified function

$$F(t, U) = \begin{cases} f(t, U) & \text{if } r_0 \leq U, \\ f^*(t, U) & \text{if } r_0 > U, \end{cases}$$

where $f^*(t, U)$ is any function such that $F(t, U)$ satisfies the global Lipchitz and growth condition. Hence by Theorem 3.1 (Mao 2007, p.51), there is a unique solution $U(t)$ in $\mathcal{M}^2([0, T]; \mathbb{R})$ to the equation

$$U(t) = U(0) + \int_0^t F(s, U(s))\mathrm{d}s + \int_0^t g(s, U(s))\mathrm{d}W(s), \quad t \in [0, T], \tag{9}$$

where T is the maximal time for which the solution exists. When $T < \infty$, the interval is $[0, T]$; when $T = \infty$, it is $[0, \infty)$. Since $U(0) > 0$, define the stopping time

$$T^* = T \wedge \inf\left\{t \in [0, T] : U(t) \leq r_0\right\}.$$

It follows from equation (9) that

$$U(t) = U(0) + \int_0^t f(s, U(s))\mathrm{d}s + \int_0^t g(s, U(s))\mathrm{d}W(s), \quad t \in [0, T^*]. \tag{10}$$

Equation (10) shows the existence of a unique solution to SM model in $\mathcal{M}^2([0, T^*]; \mathbb{R})$. Now, we show that $T^* = \infty$. Furthermore, we will show $U(t) \in \mathbb{R}_+$ for $t \geq 0$ a.s. Following the approach in (Jiang et al. 2011, Theorem 2.1), since $U(0) \in \mathbb{R}_+$, set $k_0 > 0$ sufficiently large for $U(0) \in \left[\frac{1}{k_0}, k_0\right]$. For each integer $k \geq k_0$, define the stopping time

$$\tau_k = \inf\left\{t \in [0, \tau_e) : U(t) \notin \left(\frac{1}{k}, k\right)\right\},$$

where $\tau_e = \tau_{e_1} \wedge \tau_{e_2}$, τ_{e_1} is the maximal time such that $U(t)$ is positive in $[0, \tau_{e_1})$ and τ_{e_2} is the maximal time such that $U(t)$ is not blow-up in $[0, \tau_{e_2})$. It is clear that τ_k is increasing and $\tau_k \leq \tau_e$ for each k. Set $\tau_\infty = \lim_{k\to\infty} \tau_k$, therefore $\tau_\infty \leq \tau_e \leq T^*$ a.s. If $\tau_\infty = \infty$ a.s., then $T^* = \tau_e = \infty$ a.s. and $U(t)$ is global positive solution a.s. for $t \geq 0$. If this statement is false, then there exist constants $T_1 > 0$ and $\epsilon \in (0, 1)$ such that

$$P\{\tau_\infty \leq T_1\} > \epsilon.$$

Thus, there is an integer $k_1 \geq k_0$ such that

$$P\{\tau_k \leq T_1\} > \epsilon \text{ for all } k \geq k_1.$$

Define a $\mathcal{C}^2$-function $V : \mathbb{R}_+ \to \mathbb{R}_+$ as follows

$$V(U) = U - 1 - \log U.$$

Let $k \geq k_0$ and $T_1 > 0$ be arbitrary. Applying Itô's formula, we obtain

$$\begin{aligned}
\mathrm{d}V(U) &= \left(1 - \frac{1}{U}\right)\mathrm{d}U + \frac{1}{2U^2}(\mathrm{d}U)^2 \\
&= \left(1 - \frac{1}{U}\right)\left(\left(\frac{U}{(1+\eta U)(U+\zeta)} - U\right)\mathrm{d}t + \sigma U \mathrm{d}W(t)\right) + \frac{1}{2U^2}(\sigma U)^2 \mathrm{d}t \\
&= \left[\frac{U}{(1+\eta U)(U+\zeta)} - \frac{1}{(1+\eta U)(U+\zeta)} + 1 - U + \frac{\sigma^2}{2}\right]\mathrm{d}t \\
&+ \left(1 - \frac{1}{U}\right)\sigma U \mathrm{d}W(t) \\
&\leq \left(\frac{1}{\eta\zeta} + 1 + \frac{\sigma^2}{2}\right)\mathrm{d}t + \sigma(U-1)\mathrm{d}W(t).
\end{aligned}$$

Integrating both sides from 0 to $\tau_k \wedge T_1$ and taking expectation, yields

$$\mathbb{E}[V(U(\tau_k \wedge T_1))] \leq V(U(0)) + K(\tau_k \wedge T_1), \tag{11}$$

where $K = \left(\frac{1}{\eta\zeta} + 1 + \frac{\sigma^2}{2}\right)$.

Let $\Omega_k = \{\tau_k \leq T_1\}$ for $k \geq k_1$. By our assumption, $P(\Omega_k) \geq \epsilon$. For every $\omega \in \Omega_k$, $U(\tau_k, \omega)$ equals either k or $\frac{1}{k}$, and therefore $V(U(\tau_k, \omega))$ is either $k - 1 - \log k$ or $\frac{1}{k} - 1 + \log k$. Hence

$$\mathbb{E}[V(U(\tau_k \wedge T_1))] \geq \epsilon \min\{k - 1 - \log k, \frac{1}{k} - 1 + \log k\}. \tag{12}$$

From equation (11) and equation (12), we have

$$V(U(0)) + K(\tau_k \wedge T_1) \geq \epsilon \min\{k - 1 - \log k, \frac{1}{k} - 1 + \log k\}. \tag{13}$$

Letting $k \to \infty$, we get

$$V(U(0)) + KT_1 = \infty.$$

But this contradicts our assumption that τ_∞ is finite. Therefore, we must have $\tau_\infty = \infty$. Hence, $U(t)$ does not explode in finite time or become 0 with probability 1, proving that $U(t) \in \mathbb{R}_+$ for all $t \geq 0$ a.s. □

Corollary 2 *If assumptions A1-A3 hold, then a unique global positive solution $U(t)$ exists for SDM model.*

Proof Let $h(t)$ be a positive continuous function. Letting $r_0 = -\frac{1}{2}\zeta$, $f(t, U) = \frac{U}{(1+\eta h)(\zeta+U)} - U$, and $g(t, U) = \sigma U$ in Theorem 1, and following similar steps as in Theorem 1, with the same Lyapunov function $V(U) = U - 1 - \log U$ and a slight modification of the constant $K = 2 + \frac{\sigma^2}{2}$, we conclude that there exists a unique positive solution to

$$\mathrm{d}U = \left(\frac{U}{(1 + \eta h)(\zeta + U)} - U\right)\mathrm{d}t + \sigma U\,\mathrm{d}W(t).$$

for any given $U(0) > 0$.

Now, consider the case where $U(t - \tau) = \phi(t - \tau)$ with $\phi \in \mathcal{C}([-\tau, 0])$ and $\phi(t) > 0$ for $t \in [-\tau, 0]$. There exists a unique positive solution to

$$\mathrm{d}U = \left(\frac{U}{(1 + \eta\phi(t - \tau))(\zeta + U)} - U\right)\mathrm{d}t + \sigma U\mathrm{d}W(t), \text{ in } [0, \tau],$$

with initial condition $U(0) = \phi(-\tau)$. Once the solution in $[0, \tau]$ is known, we apply the same argument iteratively in $[\tau, 2\tau]$, $[2\tau, 3\tau]$ and so on. Hence, we conclude the existence of a unique positive solution for $t \geq 0$ for a given $U(t) = \phi(t)$ in $\mathcal{C}([-\tau, 0])$. □

Remark 1 The same results for M and DM models would follow from Theorem 1 and Corollary 2, respectively, when we set $\sigma = 0$.

Next, we will prove the global existence and positivity results for the SMS model in the following theorems. First, we transform the SMS model into a matrix form. Let $\mathcal{U} = (U_1, U_2, \ldots, U_N)$, $g : [0, T] \times \mathbb{R}^N \to \mathbb{R}^{N\times N}$, and $f : [0, T] \times \mathbb{R}^N \to \mathbb{R}^N$ be defined as

$$g(t, \mathcal{U}(t)) = \text{diag}\,(\sigma_1 U_1(t), \sigma_2 U_2(t), \ldots, \sigma_N U_N(t)), \tag{14}$$
$$f(t, \mathcal{U}(t)) = (f_1, f_2, \ldots, f_N), \tag{15}$$

where $f_i : [0, T] \times \mathbb{R} \to \mathbb{R}$ are defined as

$$f_i(t, \mathcal{U}(t)) = \frac{U_i}{(1 + \eta U_i)(\zeta + U_i)} - U_i - w_{i,i}U_i + \sum_{j=1 j\neq i}^{N} w_{i,j}U_j. \tag{16}$$

Let $\mathcal{W} = (W_1, W_2, \ldots, W_N)^T$ be an N-dimensional Brownian motion, then we have the matrix form of SMS model as

$$\mathrm{d}\mathcal{U} = f(t, \mathcal{U}(t))\mathrm{d}t + g(t, \mathcal{U}(t))\mathrm{d}\mathcal{W}(t). \tag{17}$$

Theorem 3 *For any given initial value $\mathcal{U}(0) \in \mathbb{R}^N_+$, there is a unique positive solution $\mathcal{U}(t)$ to the SMS model for $t \geq 0$ and the solution will remain in $\mathbb{R}^N_+$ for all $t \geq 0$ a.s.*

Proof Consider the matrix form of SMS model

$$\mathrm{d}\mathcal{U} = f(t, \mathcal{U}(t))\mathrm{d}t + g(t, \mathcal{U}(t))\mathrm{d}\mathcal{W}(t). \tag{18}$$

It is straightforward that $g(t, \mathcal{U})$ defined in equation (14) satisfies the global Lipchitz and growth conditions of Theorem 3.1 (Mao 2007, p.51). Let $r_0 = -\frac{1}{2}\min\{\frac{1}{\eta}, \zeta\}$ and if $r_0 \leq U_i$ then

$$\begin{aligned} |f_i(\mathcal{U})| =& \left| \frac{U_i}{(1 + \eta U_i)(\zeta + U_i)} - U_i - w_{i,i}U_i + \sum_{\substack{j=1 \\ j\neq i}}^{N} w_{i,j}U_j \right|, \\ \leq& K_1 \sum_{j=1}^{N} |U_j|, \end{aligned}$$

where K_1 is some constant independent of t and $\mathcal{U}$. The above equality implies the growth condition

$$\begin{aligned} |f(t, \mathcal{U})|^2 &= |f_1(t, \mathcal{U})|^2 + |f_2(t, \mathcal{U})|^2 + \cdots + |f_N(t, \mathcal{U})|^2, \\ &\leq K_2|\mathcal{U}|^2 \leq K_2(1 + |\mathcal{U}|^2), \end{aligned}$$

where K_2 is some constant independent of t and U. Similarly, we can show that $|f(t,\mathcal{U}) - f(t,\mathcal{V})|^2 \leq K_3|\mathcal{U}-\mathcal{V}|^2$, if $r_0 \preccurlyeq \mathcal{U},\mathcal{V}$ for some constant $K_3 > 0$. Therefore, we define the modified function

$$F(t,\mathcal{U}) = \begin{cases} f(t,\mathcal{U}) & \text{if } r_0 \leq \min\limits_i\{U_i\}, \\ f^*(t,\mathcal{U}) & \text{if } r_0 > \min\limits_i\{U_i\}, \end{cases}$$

where $f^*(t,\mathcal{U})$ is any function such that $F(t,\mathcal{U})$ satisfies the global Lipchitz and growth condition. Hence by Theorem 3.1 (Mao, 2007, p. 51), there is unique solution $\mathcal{U}(t)$ in $\mathcal{M}^2\left([0,T];\mathbb{R}^N\right)$ to equation

$$\mathcal{U}(t) = \mathcal{U}(0) + \int_0^t F(s,\mathcal{U}(s))\mathrm{d}s + \int_0^t g(s,\mathcal{U}(s))\mathrm{d}\mathcal{W}(s), \quad t \in [0,T], \tag{19}$$

where T is the maximal time for which the solution exists. When $T < \infty$, the interval is $[0,T]$; when $T = \infty$, it is $[0,\infty)$. Since $U_i(0) > 0$ for $i = 1,2,3,\ldots,N$, define the stopping time

$$T^* = T \wedge \inf\left\{t \in [0,T] : U_i(t) \leq r_0 \text{ for some } i\right\}.$$

It follows from equation (19) that

$$\mathcal{U}(t) = \mathcal{U}(0) + \int_0^t f(s,\mathcal{U}(s))\mathrm{d}s + \int_0^t g(s,\mathcal{U}(s))\mathrm{d}\mathcal{W}(s), \quad t \in [0,T^*]. \tag{20}$$

Equation (20) shows the existence of a unique solution to SMS model in $\mathcal{M}^2([0,T^*];\mathbb{R}^N)$. Now, we show that $T^* = \infty$. Furthermore, $U_i(t) \in \mathbb{R}_+$ a.s. for $t \geq 0$, $i = 1,2,3,\ldots,N$.

Since $U_i(0) \in \mathbb{R}_+$, set $k_0 > 0$ sufficiently large such that $U_i(0) \in \left[\frac{1}{k_0}, k_0\right]$, for $i = 1,2,\ldots,N$. For each integer $k \geq k_0$, define the stopping time.

$$\tau_k = \inf\left\{t \in [0,\tau_e) : U_i(t) \notin \left(\frac{1}{k}, k\right) \text{ for some } i\right\},$$

where $\tau_e = \tau_{e_1} \wedge \tau_{e_2}$, τ_{e_1} is the maximal time such that $U_i(t)$ is positive in $[0,\tau_{e_1})$ for all i and τ_{e_2} is the maximal time such that $U_i(t)$ does not blow-up in $[0,\tau_{e_2})$ for all i. Set $\tau_\infty = \lim_{k\to\infty}\tau_k$, therefore $\tau_\infty \leq \tau_e \leq T^*$ a.s. If $\tau_\infty = \infty$ a.s., then $T^* = \tau_e = \infty$ a.s. and $U_i(t) \in \mathbb{R}^+$ a.s. for $t \geq 0$. To complete the proof, it is required to show that $\tau_\infty = \infty$ a.s. If this statement is false, then there exist constant $T_1 > 0$ and $\epsilon \in (0,1)$ such that

$$P\{\tau_\infty \leq T_1\} > \epsilon.$$

Thus there is an integer $k_1 \geq k_0$ such that

$$P\{\tau_k \leq T_1\} > \varepsilon, \quad \text{for all } k \geq k_1. \tag{21}$$

Now, define $V : \mathbb{R}_+^N \to \mathbb{R}_+$ as follows:

$$V(U_1, \ldots, U_N) = \sum_{i=1}^{N} (U_i - 1 - \log U_i)\,.$$

Let $k \geq k_0$ and $T_1 > 0$ be arbitrary. Applying Itô's formula to V, we get

$$\begin{aligned}
\mathrm{d}V &= \sum_{i=1}^{N} \left[\left(1 - \frac{1}{U_i}\right) \mathrm{d}U_i + \frac{1}{2U_i^2} (\mathrm{d}U_i)^2 \right] \\
&= \left[\sum_{i=1}^{N} \left(1 - \frac{1}{U_i}\right) \left(\frac{U_i}{(1+\eta U_i)(U_i+\zeta)} - U_i - \omega_{i,i} U_i + \sum_{\substack{j=1 \\ j\neq i}}^{N} \omega_{i,j} U_j \right) \mathrm{d}t \right. \\
&\quad \left. + \sum_{i=1}^{N} \left(\left(1 - \frac{1}{U_i}\right) \sigma_i U_i \mathrm{d}W_i(t) + \frac{\sigma_i^2}{2} \mathrm{d}t \right) \right] \\
&= \sum_{i=1}^{N} \left(\frac{U_i}{(1+\eta U_i)(U_i+\zeta)} - U_i - \omega_{i,i} U_i + \sum_{j=1, j\neq i}^{N} \omega_{i,j} U_j \right) \mathrm{d}t \\
&\quad + \sum_{i=1}^{N} \left(\frac{-1}{(1+\eta U_i)(U_i+\zeta)} + 1 + \omega_{i,i} - \frac{1}{U_i} \sum_{j=1, j\neq i}^{N} \omega_{i,j} U_j \right) \mathrm{d}t \\
&\quad + \sum_{i=1}^{N} (U_i - 1) \sigma_i \mathrm{d}W_i(t) + \sum_{i=1}^{N} \frac{\sigma_i^2}{2} \mathrm{d}t.
\end{aligned}$$

By noting (see Appendix B.2)

$$-\sum_{i=1}^{N} w_{i,i} U_i + \sum_{i=1}^{N} \sum_{j=1, j\neq i}^{N} w_{i,j} U_j = 0 \quad \text{and} \quad \frac{U_i}{(1+\eta U_i)(U_i+\zeta)} \leq \frac{1}{\eta\zeta},$$

and ignoring negative terms in the bound, we get

$$\mathrm{d}V \leq \sum_{i=1}^{N} \left(\frac{1}{\eta\zeta} + 1 + \omega_{i,i} + \frac{\sigma_i^2}{2} \right) \mathrm{d}t + \sum_{i=1}^{N} \sigma_i (U_i - 1) \mathrm{d}W_i(t). \tag{22}$$

Integrating both sides of equation (22) from 0 to $\tau_k \wedge T_1$ and taking expectation, we obtain

$$\begin{aligned}
\mathbb{E}[V(U_1(\tau_k \wedge T_1), \ldots, U_N(\tau_k \wedge T_1))] &\leq \mathbb{E}[(V(U_1(0), \ldots, U_N(0))] + K\mathbb{E}[\tau_k \wedge T_1], \\
&\leq V(U_1(0), \ldots, U_N(0)) + KT_1, \qquad (23)
\end{aligned}$$

where $K = \sum_{i=1}^{N} \left(\frac{1}{\eta\zeta} + 1 + w_{i,i} + \frac{\sigma_i^2}{2} \right)$. From the same argument as in Theorem 1 we conclude that $T^* = \tau_\infty = \infty$ a.s. □

Corollary 4 *If assumptions A1-A4 hold, then a unique global positive solution $U_i(t)$ for $i = 1, 2, \ldots, N$ exists for SDMS model.*

Proof We conclude the statement of this corollary with the same arguments as in Corollary 2. □

Remark 2 The same results for MS and DMS models would follow from Theorem 3 and Corollary 4, respectively, when we set $\sigma_i = 0$ for all i.

3.2 Extinction and persistence

In this section, we derive the conditions on the dimensionless parameter ζ and the volatility parameters σ or σ_i, $i = 1, 2, \ldots, N$ that govern the extinction and persistence of toxic protein concentrations in the brain. Specifically, we analyze how these parameters influence the system's stability and determine the thresholds beyond which toxic concentrations either die out over time or persist in the long run.

Theorem 5 *Assume Assumptions A1-A3 hold. Let $U \in \mathcal{M}^2([0, \infty); \mathbb{R}^+)$ be the solution to the SM model. Then,*

(1) If $2\left(\frac{1}{\zeta} - 1\right) < \sigma^2$, then $U^* = 0$ is almost surely exponentially stable.

(2) If $2\left(\frac{1}{\zeta} - 1\right) > \sigma^2$, then there exists $\delta > 0$ such that

$$\liminf_{t\to\infty} \frac{1}{t} \int_0^t U(s)\mathrm{d}s \geq \delta, \quad a.s.$$

That is, U persists a.s.

Proof **Proof for Part (1):**
Consider the SM model

$$\mathrm{d}U(t) = \left(\frac{U(t)}{(1 + \eta U(t))(U(t) + \zeta)} - U(t) \right) \mathrm{d}t + \sigma U(t)\mathrm{d}W(t).$$

Applying Itô's formula to the function $V(t, U) = \log(U)$, we get

$$\mathrm{d}V = \left(\frac{1}{(1 + \eta U(t))(U(t) + \zeta)} - 1 - \frac{\sigma^2}{2} \right) \mathrm{d}t + \sigma \mathrm{d}W(t). \tag{24}$$

Since $\frac{1}{(1+\eta U)(U+\zeta)} \leq \frac{1}{\zeta}$ for all $U > 0$, it follows

$$\mathrm{d}V \leq \left(\frac{1}{\zeta} - 1 - \frac{\sigma^2}{2} \right) \mathrm{d}t + \sigma \mathrm{d}W(t). \tag{25}$$

Integrating equation (25) from 0 to t, we get

$$\log(U(t)) - \log(U(0)) \leq \left(\frac{1}{\zeta} - 1 - \frac{\sigma^2}{2}\right)t + \sigma W(t).$$

Let $C = -\left(\frac{1}{\zeta} - 1 - \frac{\sigma^2}{2}\right) > 0$. Then,

$$\log(U(t)) - \log(U(0)) \leq -Ct + \sigma W(t).$$

Dividing by t and taking the limit as $t \to \infty$ yields

$$\limsup_{t\to\infty} \frac{\log(U(t))}{t} \leq -C + \limsup_{t\to\infty} \frac{\sigma W(t)}{t} + \limsup_{t\to\infty} \frac{\log(U(0))}{t}.$$

By the Strong Law of Large Numbers for Brownian motion, $\lim_{t\to\infty} \frac{W(t)}{t} = 0$ a.s. Thus

$$\limsup_{t\to\infty} \frac{\log(U(t))}{t} \leq -C < 0 \quad \text{a.s.}$$

Proof for part (2):

Since $\frac{1}{(1+\eta U)(U+\zeta)} \geq \frac{1}{\zeta} - \frac{1+\eta\zeta}{\zeta^2}U$ for all $U \geq 0$ (see Appendix B.2), then from equation (24) we get

$$\mathrm{d}V \geq \left(\frac{1}{\zeta} - \frac{1+\eta\zeta}{\zeta^2}U - 1 - \frac{\sigma^2}{2}\right)\mathrm{d}t + \sigma \mathrm{d}W(t). \tag{26}$$

Integrating equation (26) from 0 to t, we get

$$\log(U(t)) \geq \log(U(0)) + \left(\frac{1}{\zeta} - 1 - \frac{\sigma^2}{2}\right)t - \frac{1+\eta\zeta}{\zeta^2}\int_0^t U(s)ds + \sigma W(t). \tag{27}$$

Let

$$a = \lim_{t\to\infty} \frac{\log(U(0)) + \sigma W(t) + \left(\frac{1}{\zeta} - 1 - \frac{\sigma^2}{2}\right)t}{t} = \frac{1}{\zeta} - 1 - \frac{\sigma^2}{2} \quad \text{a.s.}$$

and $b = \frac{1+\eta\zeta}{\zeta^2}$. By Lemma 11 (see Appendix B.1),

$$\liminf_{t\to\infty} \frac{1}{t}\int_0^t U(s)\mathrm{d}s \geq \frac{a}{b} > 0, \quad \text{a.s.}$$

Therefore, the concentration $U(t)$ persists a.s. □

Theorem 6 *Let $U_i(t) \in \mathcal{M}^2([0,\infty); \mathbb{R}^+)$, $i = 1, 2, \ldots, N$ be the solution to the SMS model.*

(1) Assume Assumptions A1-A4 hold. If $\frac{1}{\zeta} - 1 > \frac{1}{N}\sum_{i=1}^{N}(\omega_{i,i} + \frac{1}{2}\sigma_i^2)$*, then there exists* $\delta > 0$ *such that*

$$\liminf_{t\to\infty} \frac{1}{t}\int_0^t \left(\sum_{i=1}^{N} U_i(s)\right) \mathrm{d}s \geq \delta > 0, \quad a.s.$$

(2) Assume Assumptions A1-A4 hold. If $\left(\frac{1}{\zeta} - 1\right) < \frac{\sigma_{min}^2}{2N}$*, then* $U_i^* = 0$ *is almost surely exponentially stable, where* $\sigma_{min} = \min\{\sigma_1, \sigma_2, \ldots, \sigma_N\}$.

Proof **Proof for part (1):**

Consider the SMS model

$$\mathrm{d}U_i(t) = \left[\frac{U_i(t)}{(1+\eta U_i(t))(U_i(t)+\zeta)} - U_i(t) - \omega_{i,i}U_i(t) + \sum_{j=1, j\neq i}^{N} \omega_{i,j}U_j(t)\right]\mathrm{d}t + \sigma_i U_i(t)\mathrm{d}W_i(t), \tag{28}$$

for $i = 1, 2, \ldots, N$.

Let $V : \mathbb{R}_+^N \to \mathbb{R}$ be defined as

$$V(\mathcal{U}(t)) = \sum_{i=1}^{N} \log(U_i(t)),$$

where $\mathcal{U}(t) = (U_1(t), U_2(t), \ldots, U_N(t))$. Applying Ito's formula to V, we get

$$\begin{aligned}\mathrm{d}V &= \sum_{i=1}^{N}\frac{1}{U_i}\mathrm{d}U_i + \frac{1}{2}\sum_{i=1}^{N}\left(-\frac{1}{U_i^2}\right)(\mathrm{d}U_i)^2 \\ &= \sum_{i=1}^{N}\left[\frac{1}{(1+\eta U_i)(U_i+\zeta)} - 1 - \omega_{i,i} + \sum_{j=1, j\neq i}^{N}\frac{1}{U_i}\omega_{i,j}U_j - \frac{\sigma_i^2}{2}\right]\mathrm{d}t + \sum_{i=1}^{N}\sigma_i\mathrm{d}W_i(t).\end{aligned} \tag{29}$$

Note that for $U_i > 0$, $i = 1, 2, 3, \ldots, N$, we have

$$\frac{1}{\zeta} - \frac{1+\eta\zeta}{\zeta^2}U_i \leq \frac{1}{(1+\eta U_i)(U_i+\zeta)} \leq \frac{1}{\zeta} \text{ and } \sum_{i=1}^{N}\sum_{j=1, j\neq i}^{N} w_{i,j}\frac{U_j}{U_i} \geq 0.$$

Using above inequalities in equation (29), yields

$$\mathrm{d}V \geq \sum_{i=1}^{N}\left[\frac{1}{\zeta} - \frac{1+\eta\zeta}{\zeta^2}U_i - 1 - \omega_{i,i} - \frac{\sigma_i^2}{2}\right]\mathrm{d}t + \sum_{i=1}^{N}\sigma_i\mathrm{d}W_i(t). \tag{30}$$

Integrating equation (30) from 0 to t, we get

$$\sum_{i=1}^{N}\log\left(U_i(t)\right) \geq \sum_{i=1}^{N}\left(\log(U_i(0)) + \sigma_i W_i(t)\right) + \sum_{i=1}^{N}\int_0^t \left(\frac{1}{\zeta} - \frac{1+\eta\zeta}{\zeta^2}U_i(s) - 1 - \omega_{i,i} - \frac{\sigma_i^2}{2}\right)\mathrm{d}s$$
$$= \sum_{i=1}^{N}\left(\log(U_i(0)) + \sigma_i W_i(t)\right) + \sum_{i=1}^{N}\left(\frac{1}{\zeta} - 1 - \omega_{i,i} - \frac{\sigma_i^2}{2}\right)t - \sum_{i=1}^{N}\frac{1+\eta\zeta}{\zeta^2}\int_0^t U_i(s)\mathrm{d}s.$$

Since (via Jensen's inequality),

$$N\log\left(\sum_{i=1}^{N}U_i\right) \geq \sum_{i=1}^{N}\log(U_i),$$

it follows that,

$$\log\left(\sum_{i=1}^{N}U_i\right) \geq \frac{1}{N}\sum_{i=1}^{N}\left(\log(U_i(0)) + \sigma_i W_i(t)\right) + \left(\frac{1}{\zeta} - 1 - \frac{1}{N}\sum_{i=1}^{N}\left(\frac{\sigma_i^2}{2} + \omega_{i,i}\right)\right)t \qquad (31)$$
$$- \frac{1+\eta\zeta}{N\zeta^2}\int_0^t\sum_{i=1}^{N}U_i(s)\mathrm{d}s.$$

Let

$$a = \lim_{t\to\infty}\frac{\frac{1}{N}\sum_{i=1}^{N}\left(\log(U_i(0)) + \sigma_i W_i(t)\right) + \left(\frac{1}{\zeta} - 1 - \frac{1}{N}\sum_{i=1}^{N}\left(\frac{\sigma_i^2}{2} + \omega_{i,i}\right)\right)t}{t},$$
$$= \frac{1}{\zeta} - 1 - \frac{1}{N}\sum_{i=1}^{N}\left(\frac{\sigma_i^2}{2} + \omega_{i,i}\right),$$

and $b = \frac{1+\eta\zeta}{N\zeta^2}$. By Lemma 11 (see Appendix B.1),

$$\liminf_{t\to\infty}\frac{1}{t}\int_0^t\sum_{i=1}^{N}U_i(t) \geq \frac{a}{b} > 0, \quad \text{a.s.}$$

Therefore, the concentration of the proteins persists at least in one region a.s.

Proof for part (2):

To prove the extinction condition, we choose the Lyapunov function as

$$V(U(t)) = \log\left(\sum_{i=1}^{N}U_i(t)\right).$$

Applying Itô's formula to V, we obtain (see Appendix C)

$$\begin{aligned} \mathrm{d}V &= \frac{1}{S}\sum_{i=1}^{N}\mathrm{d}U_i + \frac{1}{2}\left(-\frac{1}{S^2}\right)\left(\sum_{i=1}^{N}\mathrm{d}U_i\right)^2 \\ &= \frac{1}{S}\sum_{i=1}^{N}U_i\left[\frac{1}{(1+\eta U_i)(U_i+\zeta)} - 1 - \omega_{i,i} + \sum_{j\neq i}^{N}\omega_{i,j}\frac{U_j}{U_i}\right]\mathrm{d}t + \frac{1}{S}\sum_{i=1}^{N}\sigma_i U_i\,\mathrm{d}W_i(t) \\ &\quad - \frac{1}{2S^2}\sum_{i=1}^{N}\sigma_i^2 U_i^2\,\mathrm{d}t, \end{aligned} \tag{32}$$

where $S = \sum_{i=1}^{N} U_i$. Since (see Appendix B.2),

$$\frac{1}{S}\sum_{i=1}^{N}\left(-w_{i,i}U_i + \sum_{j=1,j\neq i}^{N} w_{i,j}U_j\right) = 0 \text{ and } \frac{\sigma_{\min}^2}{2N} \leq \frac{1}{2S^2}\sum_{i=1}^{N}\sigma_i^2 U_i^2.$$

Using these inequalities in the equation (32), we get

$$\begin{aligned} \mathrm{d}V &\leq \frac{1}{S}\sum_{i=1}^{N}U_i\left(\frac{1}{\zeta} - 1\right)\mathrm{d}t + \frac{1}{S}\sum_{i=1}^{N}\sigma_i U_i\mathrm{d}W_i(t) - \frac{\sigma_{\min}^2}{2N}\mathrm{d}t, \\ &\leq \left(\frac{1}{\zeta} - 1 - \frac{\sigma_{\min}^2}{2N}\right)\mathrm{d}t + \sum_{i=1}^{N}\sigma_i\mathrm{d}W_i(t). \end{aligned} \tag{33}$$

Integrating equation (33) from 0 to t, we get

$$\log\left(\sum_{i=1}^{N}U_i(t)\right) \leq \log\left(\sum_{i=1}^{N}U_i(0)\right) + \left(\frac{1}{\zeta} - 1 - \frac{\sigma_{\min}^2}{2N}\right)t + \sum_{i=1}^{N}\sigma_i W_i(t) \tag{34}$$

Dividing by t and taking the limit as $t \to \infty$, yields

$$\begin{aligned} \limsup_{t\to\infty}\frac{\log\left(\sum_{i=1}^{N}U_i(t)\right)}{t} &\leq \limsup_{t\to\infty}\frac{\log\left(\sum_{i=1}^{N}U_i(0)\right)}{t} \\ &+ \left(\frac{1}{\zeta} - 1 - \frac{\sigma_{\min}^2}{2N}\right) + \sum_{i=1}^{N}\sigma_i\limsup_{t\to\infty}\frac{W_i(t)}{t}. \end{aligned}$$

By the Strong Law of Large Numbers for Brownian motion, $\lim_{t\to\infty} \frac{W_i(t)}{t} = 0$ a.s. Thus

$$\limsup_{t\to\infty} \frac{\log\left(\sum_{i=1}^{N} U_i(t)\right)}{t} \leq \left(\frac{1}{\zeta} - 1 - \frac{\sigma_{\min}^2}{2N}\right) < 0, \text{ a.s.}$$

This implies,

$$\limsup_{t\to\infty} \frac{\log\left(U_i(t)\right)}{t} \leq \left(\frac{1}{\zeta} - 1 - \frac{\sigma_{\min}^2}{2N}\right) < 0, \text{ a.s.}$$

for $i = 1, 2, \ldots, N$. □

Remark 3 If $\zeta < \frac{1}{1+\frac{\sigma^2}{2}}$ in Theorem 5, we conclude that the solution $U(t)$ of the SM model persists in the long term. Similarly, if $\zeta < \frac{1}{1+\frac{1}{N}\sum_{i=1}^{N}\left(\omega_{i,i}+\frac{1}{2}\sigma_i^2\right)}$ in Theorem 6, we conclude that at least one component $U_i(t)$ of the solution persists in the long term.

Remark 4 If $\zeta > \frac{1}{1+\frac{\sigma^2}{2}}$ and $\zeta > \frac{1}{1+\frac{\sigma_{\min}^2}{2N}}$ in Theorem 5 and Theorem 6, respectively, we conclude that the extinction equilibria in SM and SMS models are a.s. exponentially stable. Biologically speaking, the dimensionless parameter ζ is defined as the reciprocal of the average number of PrP^{Sc} produced from single PrP^{Sc} in an initial protein population of PrP^{C}. This means that the clearance of PrP^{Sc} proteins dominates their production, causing PrP^{Sc} concentrations to decrease exponentially over time and eventually vanish. In other words, the system naturally suppresses the accumulation of misfolded proteins when ζ is sufficiently large.

If $\zeta < 1$, DM model has a positive equilibrium point given by

$$U^+ = \frac{-(1+\eta\zeta) + \sqrt{(1+\zeta\eta)^2 - 4\eta(\zeta-1)}}{2\eta}. \tag{35}$$

However, for the SM model, U^+ is no longer an equilibrium, and the stochastic solutions do not converge to U^+. Instead, we analyze the asymptotic behavior of the stochastic solutions in the vicinity of U^+.

3.3 Asymptotic analysis

Lemma 7 *Let $U \in \mathcal{M}^2([0,\infty);\mathbb{R}^+)$ be a solution to SM model. If $\sigma < \sqrt{2}$, then*

$$\limsup_{t\to\infty} \frac{1}{t}\mathbb{E}\int_0^t U^2(s)\mathrm{d}s \leq \frac{2}{\eta(2-\sigma^2)}.$$

Proof Let $V : \mathbb{R}^+ \to \mathbb{R}^+$ be the positive function defined as $V(U) = U^2$. Then

$$\mathrm{d}V = 2U\mathrm{d}U + (\mathrm{d}U)^2$$

$$= 2\Big[\frac{U^2}{(1+\eta U)(\zeta+U)} - U^2\Big]\mathrm{d}t + \sigma U^2 \mathrm{d}W(t) + \sigma^2 U^2 \mathrm{d}t$$
$$\leq \frac{2}{\eta}\mathrm{d}t + \left(\sigma^2 - 2\right) U^2 \mathrm{d}t + \sigma U^2 \mathrm{d}W(t). \tag{36}$$

Integrating equation (36) from 0 to t and then taking expectation on both sides, we get

$$0 \leq \mathbb{E}V(t) \leq \mathbb{E}V(0) + \left(\sigma^2 - 2\right)\mathbb{E}\int_0^t U^2 \mathrm{d}s + \frac{2}{\eta}t + \sigma\mathbb{E}\int_0^t U^2 \mathrm{d}W(s).$$

Since $\sigma^2 - 2 < 0$ and $\mathbb{E}\int_0^t U^2 \mathrm{d}W(s) = 0$ (Mao 2007, p.22), we have

$$\left(2 - \sigma^2\right)\mathbb{E}\int_0^t U^2 \mathrm{d}s \leq \mathbb{E}V(0) + \frac{2}{\eta}t.$$

Then,

$$\limsup_{t\to\infty} \frac{1}{t}\mathbb{E}\int_0^t U^2 \mathrm{d}s \leq \frac{2}{(2-\sigma^2)\eta}.$$

□

Theorem 8 *Let $U \in \mathcal{M}^2([0,\infty);\mathbb{R}^+)$ be the solution to SM model. If $\zeta < 1$ and $\sigma < \sqrt{2}$, then*

$$\limsup_{t\to\infty} \frac{1}{t}\mathbb{E}\int_0^t (U - U^+)^2 \mathrm{d}t \leq K\frac{\sigma^2}{(2-\sigma^2)},$$

where U^+ is the positive fixed point of the M model for some $0 < K < \infty$.

Proof Let $V : \mathbb{R} \to \mathbb{R}^+$ be the positive function defined as $V(U) = (U - U^+)^2$. Then

$$\mathrm{d}V = 2(U-U^+)\mathrm{d}U + (\mathrm{d}U)^2$$
$$= 2(U-U^+)\Big[\frac{U}{(1+\eta U)(\zeta+U)} - U\Big]\mathrm{d}t + 2U\sigma(U-U^+)\mathrm{d}W(t) + \sigma^2U^2\mathrm{d}t. \tag{37}$$

Let $f(U) = \frac{U}{(1+\eta U)(\zeta+U)} - U$. Since $f(U^+) = 0$,

$$f(U) = f(U) - f(U^+)$$
$$= \frac{U}{(1+\eta U)(\zeta+U)} - U - \frac{U^+}{(1+\eta U^+)(\zeta+U^+)} + U^+$$
$$= \frac{\zeta(U-U^+) - \eta U U^+(U-U^+)}{(1+\eta U)(\zeta+U)(1+\eta U^+)(\zeta+U^+)} - (U-U^+),$$

thus

$$f(U)(U-U^+) = \frac{\zeta(U-U^+)^2 - \eta U U^+(U-U^+)^2}{(1+\eta U)(\zeta+U)(1+\eta U^+)(\zeta+U^+)} - (U-U^+)^2$$
$$\leq \left(\frac{1}{(1+\eta U)(1+\eta U^+)(\zeta+U^+)} - 1\right)(U-U^+)^2.$$

Since $\frac{1}{(1+\eta U^+)(\zeta+U^+)} - 1 = 0$, for $U \geq 0$, we have

$$\left(\frac{1}{(1+\eta U)(1+\eta U^+)(\zeta+U^+)} - 1\right) \leq -K_1,$$

where $0 < K_1 < \infty$. Therefore,

$$\mathrm{d}V \leq -2K_1(U-U^+)^2\mathrm{d}t + 2\sigma U(U-U^+)\mathrm{d}W(t) + \sigma^2 U^2 \mathrm{d}t. \tag{38}$$

Integrating equation (38) from 0 to t and then taking expectations to both side, yields

$$0 \leq \mathbb{E}V(t) \leq \mathbb{E}V(0) - 2K_1\mathbb{E}\int_0^t (U-U^+)^2\mathrm{d}s + 2\sigma\mathbb{E}\int_0^t U(U-U^+)\mathrm{d}W(s)$$
$$+ \sigma\mathbb{E}\int_0^t U^2\mathrm{d}s.$$

Since $K_1 > 0$ and $\mathbb{E}\int_0^t U(U-U^+)\mathrm{d}W(s) = 0$ (Mao 2007, p.22), we have

$$\limsup_{t\to\infty} \frac{1}{t}\mathbb{E}\int_0^t (U-U^+)^2\mathrm{d}s \leq \frac{\sigma^2}{2K_1}\limsup_{t\to\infty}\frac{1}{t}\mathbb{E}\int_0^t U^2\mathrm{d}s.$$

Lemma 7 implies the following inequality

$$\limsup_{t\to\infty} \frac{1}{t}\mathbb{E}\int_0^t (U-U^+)^2\mathrm{d}s \leq K\frac{\sigma^2}{\eta(2-\sigma^2)},$$

where $K = \frac{1}{K_1\eta}$. □

Remark 5 This theorem demonstrates that the stochastic solution will fluctuate around the value U^+, with the intensity of these fluctuations being related to the parameter σ. If the stochastic perturbation diminishes to zero, the solution of the SM model will approach the equilibrium solution of the M model, meaning that the impact of the random fluctuations becomes negligible, and the system behaves deterministically.

3.3.1 Hopf bifurcation

In this section, we derive the conditions on parameters ζ, η, and τ, where the stability of the protein concentration changes and oscillatory behavior is observed. Consider the DM model

$$\frac{\mathrm{d}U}{\mathrm{d}t} = f(U, U_\tau), \tag{39}$$

where, $U_\tau = U(t-\tau)$ and $f(U, U_\tau) = \frac{U}{(1+\eta U_\tau)(\zeta+U)} - U$. In steady state, we have $U_\tau = U$. A straightforward calculation then gives a positive fixed point U^+, as defined in equation (35), which exists when $\zeta < 1$. If $\zeta \geq 1$, $U = 0$ is the only nonnegative fixed point. To analyze the behavior of solutions near the positive fixed point, we introduce the perturbation $V = U - U^+$, where V represents a small deviation from U^+. Then equation (39) transformed to

$$\frac{\mathrm{d}U}{\mathrm{d}t} = f(V + U^+, V_\tau + U^+). \tag{40}$$

Linearizing equation (40) using Taylor series around (U^+, U^+)

$$f(U, U_\tau) \sim f(U^+, U^+) + \frac{\partial f}{\partial U}\Big|_{(U^+,U^+)}(U - U^+) + \frac{\partial f}{\partial U_\tau}\Big|_{(U^+,U^+)}(U_\tau - U^+).$$

Therefore, we get

$$\frac{\mathrm{d}V}{\mathrm{d}t} = BV + CV_\tau, \tag{41}$$

where $B = \frac{\partial f}{\partial U}\Big|_{(U^+,U^+)} = \frac{\zeta}{(1+\eta U^+)(\zeta+U^+)^2} - 1$ and
$C = \frac{\partial f}{\partial U_\tau}\Big|_{(U^+,U^+)} = \frac{-U^+\eta}{(1+\eta U^+)^2(U^++\zeta)}$.

Let $V = \mathrm{e}^{\lambda t}$ for $\lambda \in \mathbb{C}$. Then equation (41) becomes

$$\lambda = B + C\mathrm{e}^{-\lambda\tau}. \tag{42}$$

Since a necessary condition for Hopf bifurcation is the existence of purely imaginary eigenvalues, we set $\lambda = i\omega$ in the characteristic equation (42) to get

$$i\omega = B + C(\cos(\omega\tau) - i\sin(\omega\tau)), \tag{43}$$

where $\omega \in \mathbb{R}$ and $i = \sqrt{-1}$.

The real and imaginary parts of equation (43) are given by

$$B = -C\cos(\omega\tau), \tag{44}$$
$$\omega = -C\sin(\omega\tau). \tag{45}$$

Simplifying equations (44)–(45), we find

$$\omega = \pm\sqrt{C^2 - B^2} \quad \text{and} \quad \frac{\omega}{B} = \tan(\omega\tau). \tag{46}$$

If $C^2 > B^2$, there exists a pair of complex conjugate eigenvalues $\{\pm\sqrt{C^2 - B^2}i\}$ for some τ^* such that $\frac{\omega}{B} = \tan(\omega\tau^*)$.

From the Lemma 4 of (Çalış et al. 2022), the function $F(\lambda(\tau), \tau) = \lambda - B - Ce^{-\lambda\tau}$ satisfies the transversality condition i.e., $\frac{d\mathrm{Re}(\lambda(\tau^*))}{d\tau} > 0$. By applying Lemma 5 and Remark 3 from (Çalış et al. 2022) to equation (42), we arrive at the following remark.

Remark 6 If $\zeta < 1$ and $C^2 > B^2$, then there exists a Hopf bifurcation point τ^* such that the solution of DM model is stable if $\tau \in [0, \tau^*)$ and shows the oscillatory behavior at $\tau \geq \tau^*$ where

$$\tau^* = \min\left\{\tau \in \mathbb{R}^+ : \frac{\sqrt{C^2 - B^2}}{B} = \tan(\sqrt{C^2 - B^2}\tau)\right\}.$$

If $\zeta < 1$ and $C^2 \leq B^2$, then the fixed point U^+ is asymptotically stable for all $\tau \geq 0$. Indeed, when $\tau = 0$, the characteristic root $\lambda = C + B < 0$ (see proof of Lemma 9). As τ varies, the sum of the orders of the zeros of equation (42) in the open right half-plane can change only if a zero appears on or crosses the imaginary axis (Ruan and Wei 2003).

In the following Lemma, we derive the condition on the dimensionless parameters to conclude the sign of $C^2 - B^2$.

Lemma 9 *Let* $C = \frac{-U^+\eta}{(1+\eta U^+)^2(\zeta+U^+)}$ *and* $B = \frac{\zeta}{(1+\eta U^+)(\zeta+U^+)^2} - 1$. *If* $0 < \zeta \leq \frac{1}{\eta}$, *then* $C^2 \leq B^2$, *and if* $\frac{1}{\eta} < \zeta < 1$, *then* $C^2 > B^2$.

Proof Since U^+ is a positive equilibrium point of equation (39), $f(U^+, U^+) = 0$, it follows that

$$(1 + \eta U^+)(\zeta + U^+) = 1.$$

Hence,

$$C = \frac{-U^+\eta}{1 + \eta U^+} \quad \text{and} \quad B = \frac{\zeta}{\zeta + U^+} - 1.$$

Since $C^2 - B^2 = (C + B)(C - B)$, it is sufficient to determine the signs of $C - B$ and $C + B$ to ascertain the sign of $C^2 - B^2$.

Let

$$\begin{aligned} C - B &= \frac{-U^+\eta}{1 + \eta U^+} - \frac{\zeta}{\zeta + U^+} + 1 \\ &= \frac{-U^+\eta - 1 + 1}{1 + \eta U^+} - \frac{\zeta}{\zeta + U^+} + 1 \\ &= \frac{1}{1 + \eta U^+} - \frac{\zeta}{\zeta + U^+} \\ &= 1 - \eta\zeta. \end{aligned}$$

And,

$$C + B = \frac{-U^+\eta}{1 + \eta U^+} + \frac{\zeta}{\zeta + U^+} - 1$$

$$= \frac{-U^+\eta}{1+\eta U^+} + \frac{\zeta+1-1}{\zeta+U^+} - 1$$
$$= \frac{-U^+\eta}{1+\eta U^+} - \frac{1}{\zeta+U^+} < 0.$$

Since $C + B < 0$, it follows that $C^2 - B^2$ is positive if $C - B < 0$, and nonpositive if $C - B \geq 0$. As $C - B \geq 0$ when $1 \leq \eta\zeta$, we conclude that $C^2 > B^2$ for $\frac{1}{\eta} < \zeta < 1$. Similarly, $C^2 \leq B^2$ for $0 < \zeta \leq \frac{1}{\eta}$. □

Based on Lemma 9 and Remark 6, we state the following Hopf bifurcation theorem.

Theorem 10 *If* $\frac{1}{\eta} < \zeta < 1$, *then there exists a Hopf bifurcation point* τ^* *such that solution of DM model is stable if* $\tau \in [0, \tau^*)$ *and shows the oscillatory behavior at* $\tau \geq \tau^*$ *where*

$$\tau^* = \min\left\{\tau \in \mathbb{R}^+ : \frac{\sqrt{C^2 - B^2}}{B} = \tan\left(\sqrt{C^2 - B^2}\tau\right)\right\}.$$

If $0 < \zeta \leq \frac{1}{\eta}$ *and* $\zeta < 1$, *then the fixed point* U^+ *is asymptotically stable for* $\tau \geq 0$.

Remark 7 Biologically, the Hopf bifurcation with respect to time delay can be interpreted as follows. Excess accumulation of PrP^{Sc} around neurons triggers ER stress and activation of the UPR. This response temporarily shuts down global protein translation, reducing both PrP^{C} synthesis and PrP^{Sc} production. Once PrP^{Sc} decays sufficiently, the neuron restores its normal mechanisms and resumes protein production, leading to new PrP^{C} being converted by the remaining PrP^{Sc}. This on–off mechanism of UPR can lead neurons to exhibit oscillatory behavior in PrP^{C} synthesis and PrP^{Sc} production.

4 Numerical simulations

To confirm the analytical results presented above, we numerically simulate the solutions of equations (4) and (8) using Milstein's finite difference scheme (Mil'shtein 1979). For simplicity, we begin with arbitrary initial data and parameters that satisfy the conditions for persistence, extinction, and bifurcation. Our numerical results are consistent with the theoretical predictions presented in the previous section. Finally, we simulate the spread of toxic protein across the brain using a biologically informed network, and the resulting time series of U for different parameter sets are summarized in Table 4.

4.1 Parameter variation

In the previous section, we theoretically established the influence of model parameters on toxic protein behavior. To further examine this, we performed a sensitivity analysis by systematically varying key parameters τ, ζ, and η, as shown in Fig. 2. The analysis

Table 4 Overview of numerical results and their theoretical implications

Numerical result	Interpretation
Fig. 2	Illustrates the sensitivity of the model to key parameters.
Fig. 3 and Fig. 4	Numerical results validate Theorem 5; the chosen parameters satisfy the conditions for extinction and persistence.
Fig. 5a and Fig. 5b	Numerical simulations validate Theorem 10; the selected parameters satisfy the hypotheses for a Hopf bifurcation.
Fig. 6 and Fig. 7	Illustrate the effect of stochastic perturbations on the deterministic solution.
Fig. 8 and Fig. 9	Numerical results validate Theorem 5 for the connectome model. For visualization, three arbitrarily chosen brain regions are considered, connected through an arbitrary connectome matrix.
Fig. 11 and Fig. 12	Illustrate the spatiotemporal spread of toxic protein across the brain using clinical parameters and a real connectome matrix.

shows that the main behaviors–extinction, persistence, and oscillations–are preserved across a range of biologically relevant values. In particular, oscillatory dynamics consistently appear for sufficiently large delays and remain stable under moderate changes in ζ and η. This indicates that the observed dynamics are not dependent on a single parameter choice, highlighting the robustness and empirical relevance of the model predictions. The detailed sensitivity analysis is provided in Section 4.5.1.

4.2 Extinction and persistence for the scalar model

By Theorem 5, we established that the toxic protein concentration persists a.s. in the long term if

$$\zeta < \frac{1}{1+\frac{\sigma^2}{2}}, \tag{47}$$

whereas it goes extinct a.s. if

$$\zeta > \frac{1}{1+\frac{\sigma^2}{2}}. \tag{48}$$

We consider a set of parameters that satisfy equations (47)–(48) and conduct numerical simulations to validate the theoretical predictions outlined in the previous section. In Fig. 3, we select parameters that satisfy the persistence condition given by equation (47). The numerical simulations show that the concentration of the toxic protein remains sustained over time, aligning with the theoretical expectation that persistence occurs when these conditions are met. Since equation (47) is independent of η, we choose $\eta = 2, 5, 10$ arbitrarily. In Fig. 4, we investigate the extinction scenario by selecting parameter values that satisfy the extinction condition given in equation (48). The numerical results illustrate that, under these conditions, the toxic protein concentration gradually declines over time and eventually vanishes. This observation

Fig. 2 Toxic protein dynamics for different parameters σ, ζ, η and τ. This figure illustrates the robustness of the model dynamics and how the protein concentration evolves under varying stochastic and biological conditions

confirms the theoretical prediction that extinction occurs when ζ and σ satisfy equation (48). Overall, our numerical findings provide strong empirical support for the theoretical results derived in the previous section. By demonstrating both the persistence and extinction dynamics through computational experiments, we establish a comprehensive understanding of the conditions governing the long-term behavior of the system.

4.3 Hopf bifurcation

We present time series plots of the dependent variable U for various values of the time delay τ, which induce oscillatory behavior in the delayed deterministic model, as predicted by Theorem 10. Fig. 5a depicts the case where the parameters are set to $\zeta = 0.21$ and $\eta = 10$, which satisfy the bifurcation criterion $(\frac{1}{\eta} < \zeta < 1)$ as detailed in Theorem 10. The initial condition is set as $U(0) = 0.5$, with the history function defined by $\phi(t) = 0.5$ for $t \in [-\tau, 0]$. The positive imaginary part of the eigenvalue is found to be $\omega = 0.4327$, and the critical delay value is calculated from

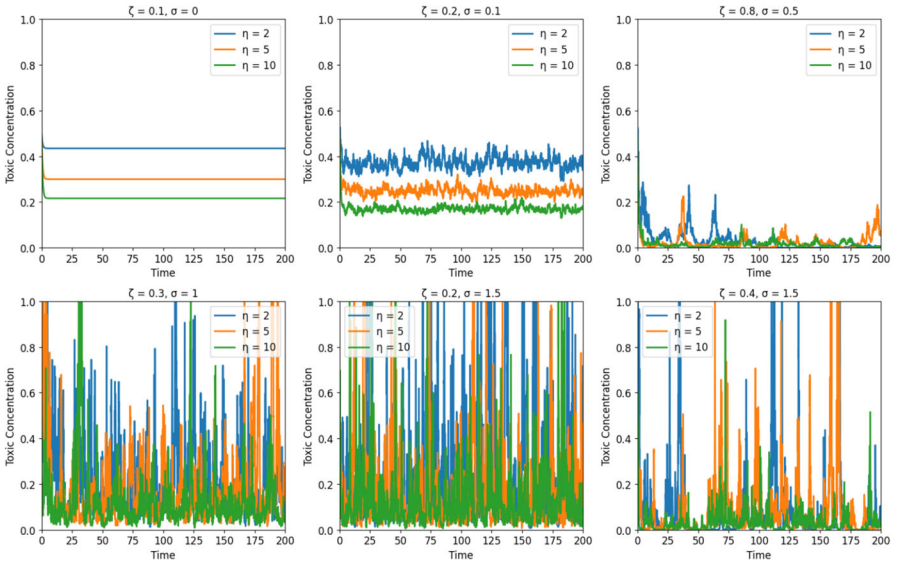

Fig. 3 Numerical solution of equation (4) showing toxic protein persistence. Parameters ζ and σ satisfy the condition $\zeta < \frac{1}{1+\frac{\sigma^2}{2}}$

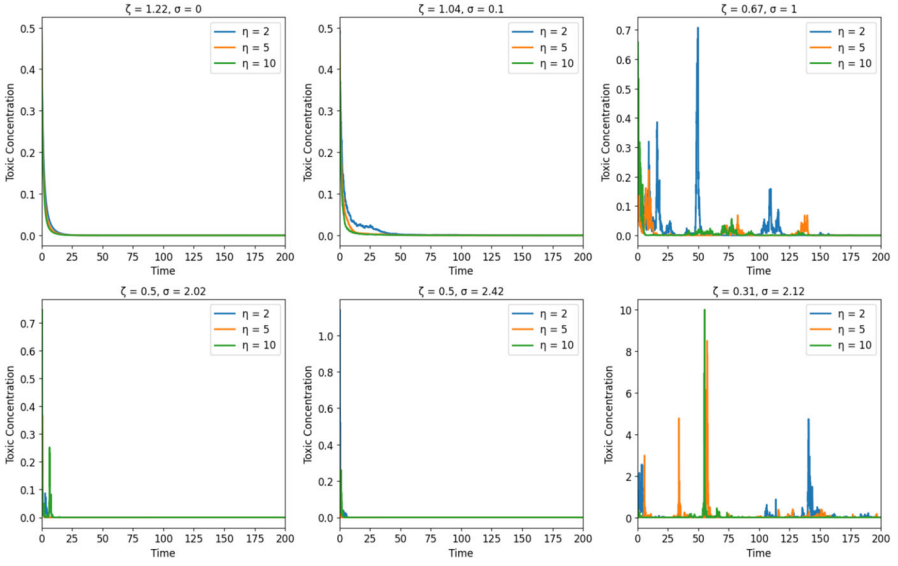

Fig. 4 Numerical solution of equation (4) showing toxic protein extinction. Parameters ζ and σ satisfy the condition $\zeta > \frac{1}{1+\frac{\sigma^2}{2}}$.

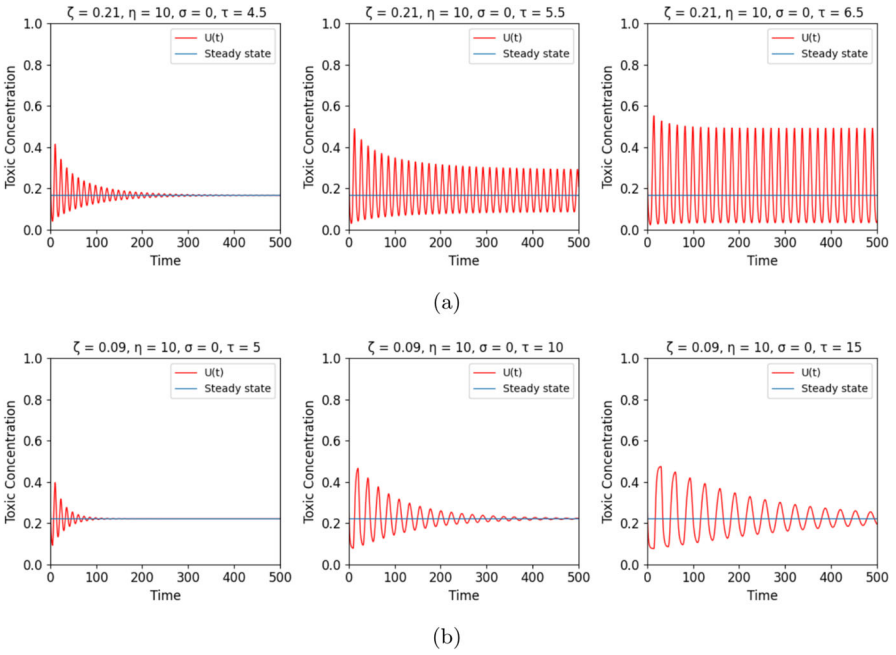

Fig. 5 Numerical solution of equation (4) with $\sigma = 0$: (a) For $\zeta = 0.21$ and $\eta = 10$, the system undergoes a Hopf bifurcation at $\tau \sim 5.5064$, leading to oscillatory behavior. (b) For $\zeta = 0.09$ and $\eta = 10$, the Hopf bifurcation condition is not satisfied, resulting in no periodic evolution

equation (46) as $\tau^* = 5.5064$. As shown in Fig. 5a, for $\tau > \tau^*$, the system exhibits sustained oscillatory behavior, whereas for $\tau < \tau^*$ the oscillations decay over time.

In Fig. 5b, we consider a different parameter set with $\zeta = 0.09$ and $\eta = 10$, which does not satisfy the Hopf bifurcation criterion. As predicted by the theoretical analysis in Theorem 10, Fig. 5b demonstrates the absence of periodic behavior for the selected time delays $\tau = 5$, 10, and 15, consistent with the lack of sustained oscillations in this case.

4.3.1 Effect of stochasticity

In Theorem 8, we established that the root mean squared value of $U - U^+$ remains bounded under the conditions $\zeta < 1$ and $\sigma < \sqrt{2}$. Specifically, this boundedness exhibits a direct proportionality to σ, implying that as σ decreases, the fluctuations around the equilibrium point U^+ also diminish. We present numerical simulations of the SM model to validate these theoretical findings, as illustrated in Fig. 6. The results demonstrate that for higher values of σ, the deviation from U^+ is more pronounced, whereas for smaller values of σ, the fluctuations are significantly reduced. These computational results confirm that the stochastic perturbations governed by σ play a critical role in determining the stability and long-term behavior of the system.

In Theorem 10, we analyzed the Hopf bifurcation for the deterministic model. While the introduction of stochasticity may alter the bifurcation condition, a detailed

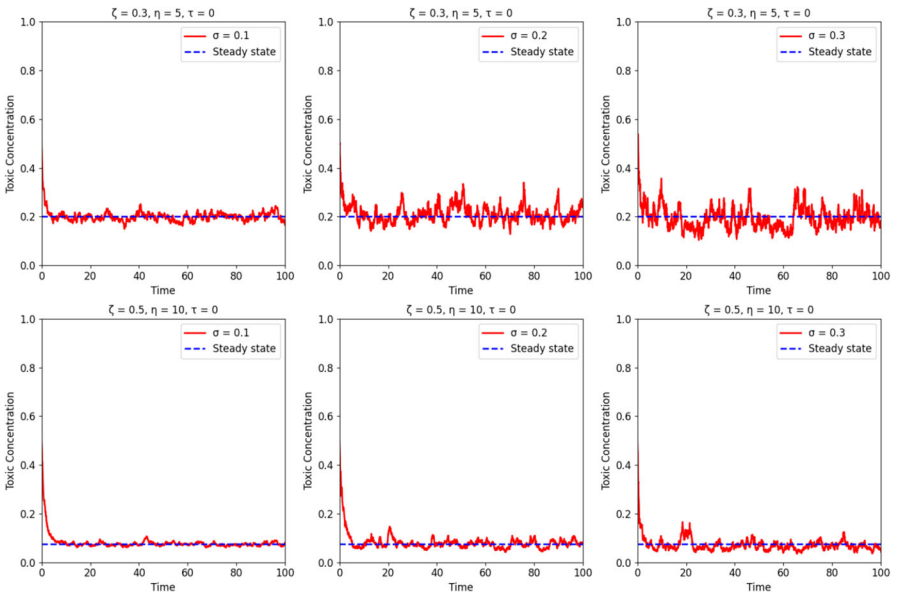

Fig. 6 Numerical solution of equation (4)–Asymptotic behavior of the stochastic solution around the equilibrium point U^+. As the stochastic perturbation decreases, fluctuations around the equilibrium point also decrease (right to left)

analysis of this effect is left for future work. Nevertheless, in Theorem 8, we establish that, in the absence of time delay, the mean-square deviation of the stochastic solution from the fixed point U^+ decreases as the noise intensity σ decreases. This suggests that the Hopf bifurcation results obtained for the deterministic model may remain valid under small stochastic perturbations. In Fig. 7, we examine three sets of parameter values, ζ and η, which result in Hopf bifurcation points at $\tau^* = 8.2$, $\tau^* = 21.57$, and $\tau^* = 6.01$, presented from top to bottom, respectively. The Hopf bifurcation points are determined using equation (46) for the deterministic case when $\sigma = 0$. When introducing small stochastic perturbations, specifically $\sigma = 0.01$ and $\sigma = 0.05$, the stochastic solutions exhibit behavior similar to the deterministic solution. In this regime, the Hopf bifurcation characteristics remain consistent with the results stated in Remark 6. However, as the stochastic perturbation σ increases further, the solution progressively deviates from the deterministic trajectory. This deviation becomes more pronounced, affecting the stability and periodic nature of the bifurcation. The influence of larger stochastic perturbations on the system dynamics is illustrated in Fig. 7, where the increasing randomness disrupts the regular periodic oscillations observed in the deterministic case.

4.4 Extinction and persistence for the connectome model

For simplicity, we begin our numerical experiments by considering a small synthetic system of 3 regions R_1, R_2 and R_3 with parameters chosen to illustrate Theorem 6. Then, SMS model in equation (8) simplifies to

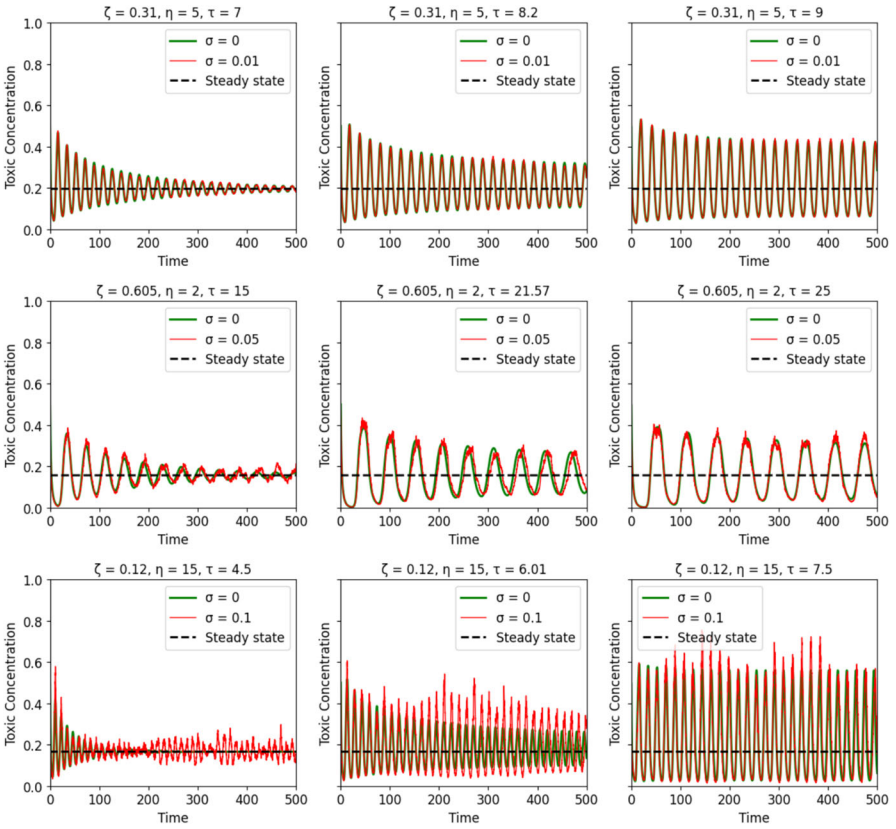

Fig. 7 Numerical solution of equation (4)- Effect of the stochastic parameter σ on oscillations. For $\sigma = 0.01$ (top row), the SDM model exhibits Hopf bifurcation behavior similar to DM model. As σ increases (top to bottom), stochastic perturbations amplify fluctuations in the oscillations

$$\mathrm{d}U_i(t) = \left[\frac{U_i(t)}{(1+\eta U_i(t))\,(\zeta + U_i(t))} - U_i(t) - \omega_{i,i}U_i + \sum_{j=1, j\neq i}^{3} \omega_{i,j}U_j\right]\mathrm{d}t + \sigma U_i \mathrm{d}W_i(t), \tag{49}$$

for i = 1,2,3. We take $\omega \in \mathbb{R}^{3\times 3}$ as

$$\omega = \begin{bmatrix} 0.4 & 0.2 & 0.2 \\ 0.1 & 0.3 & 0.5 \\ 0.3 & 0.1 & 0.7 \end{bmatrix}.$$

In Section 4.5, we then simulate the model dynamics using a biologically informed connectome matrix derived from clinical data.

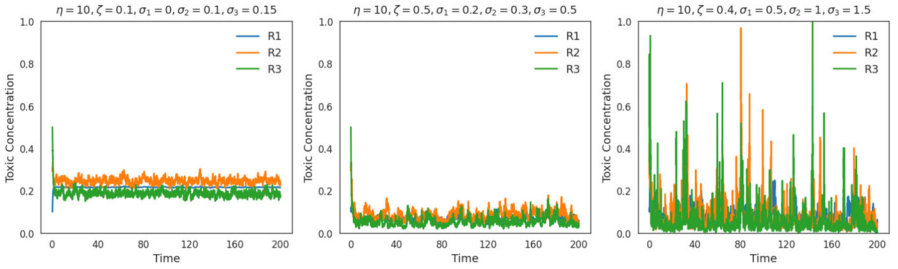

Fig. 8 Numerical solution of equation (49) showing toxic protein persistence. Parameters ζ, σ_1, σ_2, and σ_3 satisfy the condition in equation (50)

In Theorem 6, we established that the concentration of the toxic protein persists in at least one region in the long term if

$$\zeta < \frac{1}{1 + \frac{1}{N}\sum_{i=1}^{N}\left(\omega_{i,i} + \frac{1}{2}\sigma_i^2\right)}, \tag{50}$$

whereas the toxic protein concentration becomes extinct in the brain a.s. if

$$\zeta > \frac{1}{1 + \frac{\sigma_{\min}^2}{2N}}. \tag{51}$$

To support the theoretical results stated in Theorem 6, we select parameter values satisfying equations (50)–(51) and perform numerical simulations. We consider the initial toxic concentrations as $U_1(0) = 0.1$, $U_2(0) = 0.3$, and $U_3(0) = 0.5$, and assign noise intensities σ_1, σ_2, and σ_3 to regions R_1, R_2, and R_3, respectively. In Fig. 8, we select parameters that satisfy the persistence condition given in equation (50). The numerical results show that the toxic protein concentration remains sustained over time whenever the parameters satisfy this condition. Fig. 9 presents the extinction scenario, where parameter values are chosen to satisfy the condition stated in equation (51). The simulation results demonstrate that, under these conditions, the concentration of toxic protein steadily decreases over time and ultimately vanishes almost surely. These numerical results are consistent with the theoretical predictions presented in Theorem 6. Numerical results suggest that delay induces Hopf bifurcations in the SDMS model (see Appendix G). However, due to the system's complexity and strong nonlinearity, a detailed Hopf bifurcation analysis is deferred to future work.

4.5 Numerical simulation with biological data

To simulate the spatial spread of prion pathology in the brain, we constructed a connectivity matrix following the approach of (Fornari et al. 2020), using the Budapest Reference Connectome v3.0 (Szalkai et al. 2015) with minimum edge confidence 1%. The graph $\mathcal{G}$ derived from the Budapest Reference Connectome v3.0 project consists of

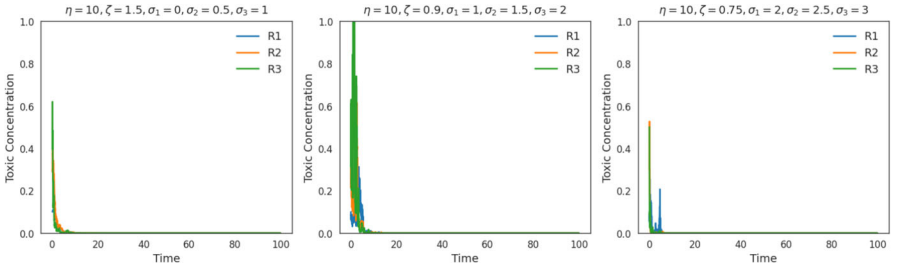

Fig. 9 Numerical solution of equation (49) showing toxic protein extinction. Parameters ζ, σ_1, σ_2, and σ_3 satisfy the condition in equation (51)

$N = 1015$ nodes and $E = 37{,}477$ weighted edges, with the mean fiber number ranging from $1 \leq n_{ij} \leq 154.8$ and the mean fiber length from 10.25 mm $\leq l_{ij} \leq$ 139.74 mm. This graph is subsequently mapped onto a reduced graph with $N = 83$ nodes and $E = 1130$ edges. Further details of node indices and their corresponding regions can be found in (Fornari et al. 2020) and its supplementary material. The edge weight between nodes i and j is defined as the ratio of the mean fiber number n_{ij} to the fiber length l_{ij}. The network consisting of 83 nodes and its weighted adjacency matrix are shown in Fig. 10. To capture the progression of toxic proteins across the whole brain network, we compute the concentration of toxic protein $U_i(t)$ at each node $i = 1, 2, \ldots, N$ as a function of time using equation (8). Following the approach of (Fornari et al. 2020; Shaheen et al. 2023), for visualization and further analysis, each node is assigned to a major anatomical region of the brain, including the temporal, parietal, frontal, basal ganglia, occipital, limbic, and brain stem regions. We then evaluate the regional mean concentration of toxic protein by averaging over all nodes belonging to each region. The averaging is defined as

$$M_j(t) = \frac{1}{x_j} \sum_{i \in \mathcal{X}_j} U_i(t), \quad j = 1, 2, \ldots, 7,$$

where $\mathcal{X}_j$ denotes the set of nodes contained in region j, and x_j is the cardinality of $\mathcal{X}_j$.

We explain the estimation of other biological parameters in Appendix F, and they are listed in Table 5.

Now we examine the spreading behavior of toxic proteins across the entire brain network by seeding an initial concentration of 1.3×10^{-5} g cm^{-3} at the brain stem, as shown in Fig. 11. This choice of both the initial concentration and the seeding location is explained in Appendix F. Accordingly, in our numerical simulations, the node corresponding to the brain stem was initialized with a concentration of 1.3×10^{-5} g cm^{-3}, while the remaining nodes in the network were initialized with zero concentration. Fig. 11 illustrates that the toxic concentration first accumulates in the seeding region and then spreads to adjacent nodes via network-mediated transport along structural connections. One can also choose a region of interest as the initial seeding position and study the dynamics of prions in the brain. The trajectories across the nodes do

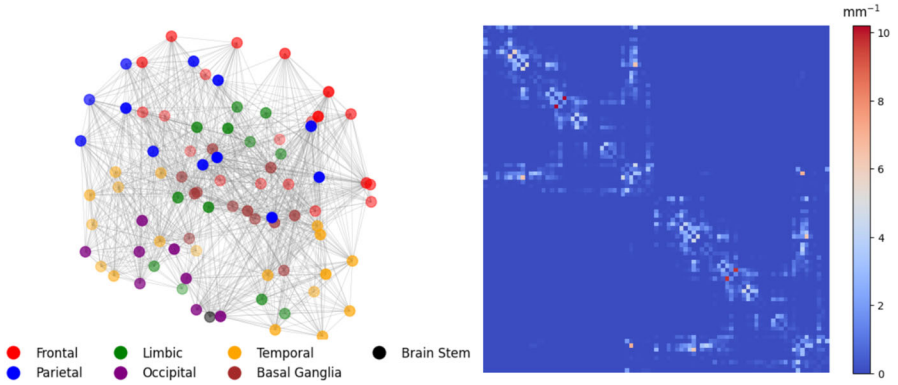

Fig. 10 Left: Three-dimensional view of the brain with its seven associated regions. Right: Weighted adjacency matrix with 83 nodes, obtained from the Budapest Reference Connectome v3.0. The color scale ranges from low weights (blue) to high weights (red), indicating strong connections between nodes

Table 5 Loose estimates of parameter values

Parameter	Value	Reference
α	$5 \times 10^{-5}\ \mathrm{s}^{-1}$	(Miller et al. 2024)
β	$3 \times 10^{-7}\ \mathrm{s}^{-1}$	(Miller et al. 2024)
γ	$2\ \mathrm{cm}^3\ \mathrm{g}^{-1}\ \mathrm{s}^{-1}$	(Miller et al. 2024)
A	$5 \times 10^{-11}\ \mathrm{g\,cm}^{-3}\ \mathrm{s}^{-1}$	(Miller et al. 2024)
t_d	$8 \times 10^4 \mathrm{s}$	(Miller et al. 2024)
$\max_{i,j}\{L_{i,j}\}$	$1 \times 10^2\ \mathrm{cm}^{-1}$	(Szalkai et al. 2015)
Y_c	$3 \times 10^{-4}\ \mathrm{g\,cm}^{-3}$	Estimated
r	$6 \times 10^{-8}\ \mathrm{cms}^{-1}$	Estimated
$\rho_{Y,i}, i = 1, 2, \ldots, N$	$3 \times 10^{-4}\ \mathrm{s}^{-1/2}$	Estimated

not intersect, indicating that the toxicity at each node evolves mostly independently without changing its ordering (see Fig. 11 (left)). Once the toxic load reaches a critical threshold, the disease process activates: the affected nodes begin producing additional toxic seeds, which then spread to neighboring nodes connected to them. This leads to secondary infections and cascading spread across the network. Because the brain network exhibits small-world characteristics (Fornari et al. 2020), such connectivity naturally accelerates the spread of toxicity, causing most nodes to become infected within a short time. Introducing stochasticity into the system accounts for the inherent variability and uncertainty in biological processes, such as protein misfolding and clearance mechanisms. With noise, the trajectories of misfolded protein concentration at each node exhibit fluctuations around their deterministic trends, reflecting the inherent randomness in inter-neuronal propagation and other stochastic biological processes. These fluctuations can lead to variability in the timing and magnitude of regional toxic load, which may explain why some brain regions show early onset of

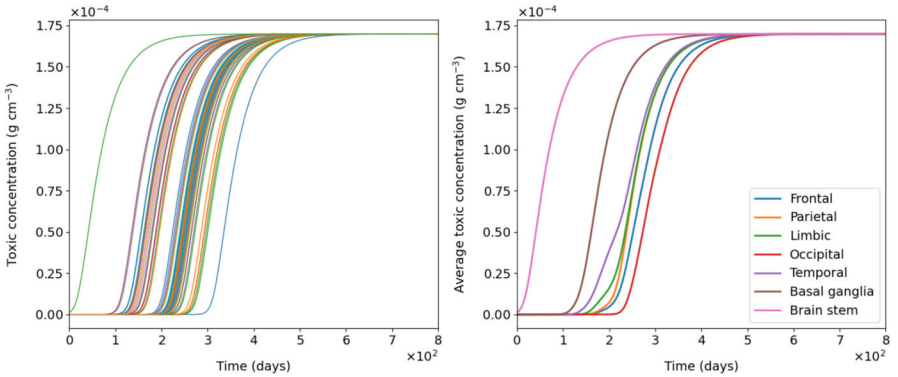

Fig. 11 Spreading behavior of toxic protein over the entire brain connectome without noise ($\rho_{Y,i} = 0\,\mathrm{s}^{-\frac{1}{2}}$ for $i = 1, 2, ..., 83$). Left: Toxic protein concentration at each node (83 nodes). Right: Average toxic concentration for seven macro regions. Parameters are given in Table 5

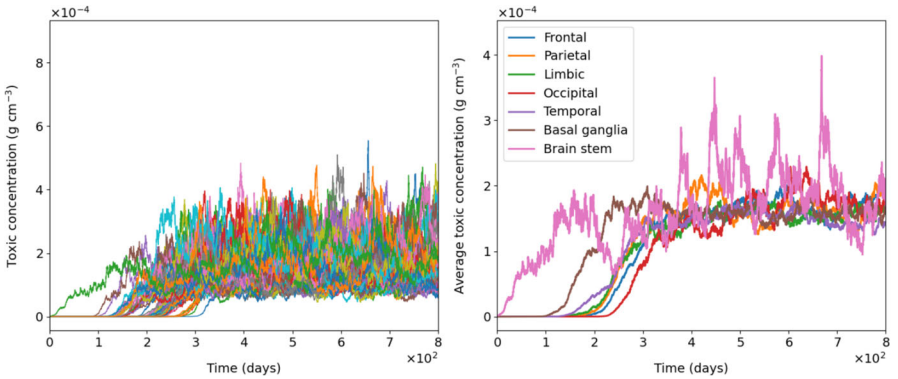

Fig. 12 Spreading behavior of toxic protein across the brain connectome with stochastic fluctuations ($\rho_{Y,i} = 3\times10^{-4}\,\mathrm{s}^{-\frac{1}{2}}$ for $i = 1, 2, ..., 83$). Left: Toxic protein concentration at each node (83 nodes). Right: Average toxic concentration for seven macro regions. Parameters are given in Table 5

pathology while others are delayed, even under similar connectivity. In Fig. 12, the trajectories no longer evolve smoothly but show small deviations that remain bounded, indicating that the overall disease spread pattern is robust but subject to stochastic modulation. Biologically, this suggests that while network structure drives the general spread of toxicity, intrinsic fluctuations can influence the precise spatiotemporal pattern of pathology, potentially accounting for patient-to-patient variability in disease progression.

4.5.1 Sensitivity analysis

The model parameters play a critical role in determining the long-term dynamics of the system. We therefore consider the clinically relevant parameters α, β, γ, Y_c, t_d, ρ_Y, and A to perform a sensitivity analysis of the connectome-based model. These

Table 6 Values of $\mathcal{M}$ at various parameter changes

Parameter	$\mathcal{M}$ g cm^{-3}
Baseline	9.20×10^{-7}
$\alpha \leftarrow 1.1\alpha$	$8.68 \times 10^{-7}(-5.6\%)$
$\alpha \leftarrow 0.9\alpha$	$9.72 \times 10^{-7}(+5.7\%)$
$\beta \leftarrow 1.1\beta$	$8.71 \times 10^{-7}(-5.3\%)$
$\beta \leftarrow 0.9\beta$	$9.64 \times 10^{-7}(4.8\%)$
$\gamma \leftarrow 1.1\gamma$	$9.62 \times 10^{-7}(4.6\%)$
$\gamma \leftarrow 0.9\gamma$	$8.58 \times 10^{-7}(-6.7\%)$
$A \leftarrow 1.1A$	$9.59 \times 10^{-7}(4.3\%)$
$A \leftarrow 0.9A$	$8.72 \times 10^{7}(-5.2\%)$
$t_d \leftarrow 1.1t_d$	$9.20 \times 10^{-7}(0.0\%)$
$t_d \leftarrow 0.9t_d$	$9.20 \times 10^{-7}(0.0\%)$
$\rho \leftarrow 1.1\rho$	$9.22 \times 10^{-7}(0.3\%)$
$\rho \leftarrow 0.9\rho$	$9.16 \times 10^{-7}(-0.4\%)$
$Y_c \leftarrow 1.1Y_c$	$9.26 \times 10^{-7}(0.7\%)$
$Y_c \leftarrow 0.9Y_c$	$9.05 \times 10^{-7}(-1.6\%)$
$r \leftarrow 1.1r$	$9.20 \times 10^{-7}(0.0\%)$
$r \leftarrow 0.9r$	$9.20 \times 10^{-7}(0.0\%)$

parameters influence toxic protein production, clearance, aggregation, stochastic variability, and delayed cellular responses, which are key mechanisms underlying prion disease progression. For the sensitivity analysis, we define the metric

$$\mathcal{M} = \mathbb{E}\big[\mathbf{Y}(\mathbb{T})\big],$$

where

$$\mathbf{Y}(\mathbb{T}) = \frac{1}{83}\sum_{i=1}^{83} Y_i(\mathbb{T}), \quad Y_i(\mathbb{T}) = \overline{Y}\, U_i(\mathbb{T}), \quad i = 1, 2, \ldots, 83.$$

Here, $\mathbf{Y}(\mathbb{T})$ represents the mean concentration of toxic protein across all brain regions at time $\mathbb{T}$. We choose $\mathbb{T} = 33$ days p.i., as experimental studies have reported that animals begin to exhibit observable clinical symptoms approximately 33 days p.i. (Beekes et al. 1996). Biologically, this metric quantifies the average toxic protein burden across all brain regions at a clinically relevant time point. It provides a global measure of disease severity by capturing the cumulative effect of protein misfolding, spread, and accumulation throughout the brain network.

For the baseline configuration, we adopt the parameter values listed in Table 5. Each parameter is then perturbed individually by $\pm 10\%$, while all remaining parameters are held fixed at their baseline values. The corresponding sensitivity analysis results are reported in Table 6. We observed that the parameters α, β, γ, and A had a substantial impact on the model dynamics, whereas the remaining parameters had comparatively minor effects.

5 Biological implications

The theoretical and computational analyses illustrate the intricate dynamics governing prion protein behavior under the influence of the dimensionless parameters ζ and η within our deterministic, stochastic, and delayed modeling frameworks. Notably, when $\zeta > 1$, all models consistently predict the extinction of toxic misfolded protein. The parameter ζ represents the reciprocal of the average number of PrP^{Sc} produced from a single PrP^{Sc} in an initial protein population of PrP^{C}. This implies that when the clearance rate is sufficiently high relative to production, the system achieves effective elimination of toxic protein species, which results in the extinction of toxic proteins in the long term. Conversely, when $\zeta < 1$, deterministic models predict either convergence to a positive equilibrium or oscillatory behavior around the equilibrium due to the time lag in the UPR. This indicates that the production of toxic misfolded protein exceeds its clearance, resulting in its sustained presence in the brain. Meanwhile, stochastic models account for biological fluctuations, capturing the inherent randomness in protein dynamics. In these models, even when the production rate of toxic misfolded proteins exceeds the clearance rate ($\zeta < 1$), stochastic effects may still lead to their eventual extinction.

6 Conclusion

In this paper, we introduced the UPR and stochasticity into heterodimer models of prion diseases, used an asymptotic scaling argument to simplify the governing dynamics, and investigated both scalar and connectome-based models. Given that biological models are highly sensitive to parameters in the long term, this study is primarily dedicated to establishing the global existence of a positive solution and deriving conditions on the parameters that govern the dynamics of the toxic protein concentration. Additionally, we investigated the oscillatory behavior of the deterministic model by considering time delay as the Hopf bifurcation parameter.

In this paper, we modeled intrinsic, small, and continuous fluctuations in the system using a Wiener process. While this choice provides a tractable framework for capturing stochastic effects, future work will focus on developing the mathematical theory under alternative noise structures, such as Lévy noise, which may better represent heavy-tailed or jump-driven dynamics. Additionally, we analyzed the asymptotic behavior of solutions to equation (4) in the neighborhood of the positive fixed point U^{+}. Due to the increased complexity of equation (8), a comprehensive stability analysis and Hopf bifurcation study for this system are deferred to future investigations.

Appendix A: Notations

In Table 7, we list all the notations used in the paper.

Table 7 Notations and Definitions

Notation	Definition
a.s.	Almost Surely
$a \vee b$	Maximum of a and b
$a \wedge b$	Minimum of a and b
$\mathbb{R}^N$	N-dimensional Euclidean space
$\mathbb{R}^N_+$	$\{x \in \mathbb{R}^N : x_i > 0,\ 1 \le i \le N\}$
$\lvert x \rvert$	Euclidean norm of vector x
$x \preccurlyeq y$	Vector x is element-wise smaller than or equal to vector y
$r_0 \preccurlyeq x$	Real number r_0 is less than or equal to each element of vector x
$\mathbb{E}$	Expected value
$\mathcal{C}(A; B)$	Space of continuous functions mapping A into B
$\mathcal{L}^p([a, b]; \mathbb{R}^N)$	$\mathbb{R}^N$-valued $\mathcal{F}_t$-adapted processes $\{f(t)\}_{a \le t \le b}$ such that $\int_a^b \lvert f(t)\rvert^p \, \mathrm{d}t < \infty$ a.s.
$\mathcal{M}^p([a, b]; \mathbb{R}^N)$	Processes $\{f(t)\}_{a \le t \le b}$ in $\mathcal{L}^p$ such that $\mathbb{E}\int_a^b \lvert f(t)\rvert^p \, \mathrm{d}t < \infty$
$(\Omega, \mathcal{F}, P)$	Probability space with filtration $\{\mathcal{F}_t\}_{t \ge 0}$, increasing and right-continuous, with $\mathcal{F}_0$ containing all P-null sets
$\mathcal{U}(t)$	$\mathbb{R}^N$-valued stochastic process $\mathcal{U}(t) = (U_1(t), \ldots, U_N(t))$ with index $t \in \mathbb{R}_+$
$W(t)$	One-dimensional Brownian motion on $(\Omega, \mathcal{F}, P)$
$\mathcal{W}(t)$	N-dimensional Brownian motion $\mathcal{W}(t) = (W_1(t), \ldots, W_N(t))$ on $(\Omega, \mathcal{F}, P)$

Appendix B: Supporting definitions and results

Definition 1 (Almost Sure Exponential Stability)(Mao 2007, p.199)

The solution $\mathcal{U}(t)$ of an N-dimensional stochastic differential equation is said to be almost surely exponentially stable at $\mathcal{U}(t) = 0$ if

$$\limsup_{t \to \infty} \frac{1}{t} \log |\mathcal{U}(t; t_0, \mathcal{U}_0)| < 0, \ \text{a.s.} \tag{B1}$$

for all $\mathcal{U}(t_0) = \mathcal{U}_0 \in \mathbb{R}^N$.

We employ the strong law of large numbers for Brownian motion $W(t)$ in most of our analyses. This law states that

$$\lim_{t\to\infty} \frac{W(t)}{t} = 0, \text{ a.s.} \tag{2}$$

which implies that, almost surely, the time-averaged Brownian motion vanishes asymptotically as $t \to \infty$.

B.1 Itô's formula

Let $\mathcal{U}$ be an N-dimensional diffusion process on $t \geq 0$ with the stochastic differential

$$\mathrm{d}\mathcal{U}(t) = f(t, \mathcal{U}(t))\mathrm{d}t + g(t, \mathcal{U}(t))\mathrm{d}\mathcal{W}(t),$$

where $f \in \mathcal{L}^1([0,\infty); \mathbb{R}^N)$ and $g \in \mathcal{L}^2([0,\infty); \mathbb{R}^{N\times N})$.
Denote by $C^{1,2}\left([0,\infty) \times \mathbb{R}^N; \mathbb{R}\right)$ the family of functions defined on $[0,\infty)\times\mathbb{R}^N$ such that they are once continuously differentiable in t and twice continuously differentiable in x. Let $V \in C^{1,2}([0,\infty) \times \mathbb{R}^N; \mathbb{R})$. Then $V(t, \mathcal{U}(t))$ is again an Itô process with the stochastic differential given by

$$\begin{aligned}\mathrm{d}V(t,\mathcal{U}(t)) = &\left[\frac{\partial V}{\partial t}(t,\mathcal{U}(t)) + \frac{\partial V}{\partial \mathcal{U}}(t,\mathcal{U}(t))f(t) + \frac{1}{2}\mathrm{trace}\left(g(t)^T \frac{\partial^2 V}{\partial \mathcal{U}^2}(t,\mathcal{U}(t))g(t)\right)\right]\mathrm{d}t \\ &+ \frac{\partial V}{\partial \mathcal{U}}(t,\mathcal{U}(t))g(t)\mathrm{d}\mathcal{W}(t), \quad \text{a.s.}\end{aligned}$$

where $\mathcal{U}(t) = (U_1(t), U_2(t), \ldots, U_N(t))^T$ and $\mathcal{W}(t) = (W_1(t), W_2(t), \ldots, W_N(t))^T$.
Let us now formally introduce a multiplication

$$\mathrm{d}t\,\mathrm{d}t = 0, \quad \mathrm{d}W_i\,\mathrm{d}t = 0, \quad \mathrm{d}W_i\,\mathrm{d}W_i = \mathrm{d}t, \quad \mathrm{d}W_i\,\mathrm{d}W_j = 0 \quad \text{if } i \neq j.$$

Moreover, the Itô formula can be written as (Mao 2007, p.36)

$$\mathrm{d}V(t,\mathcal{U}(t)) = \frac{\partial V}{\partial t}(t,\mathcal{U}(t))\mathrm{d}t + \frac{\partial V}{\partial \mathcal{U}}(t,\mathcal{U}(t))\mathrm{d}\mathcal{U} + \frac{1}{2}\mathrm{d}\mathcal{U}^T \frac{\partial^2 V}{\partial \mathcal{U}^2}(t,\mathcal{U}(t))\mathrm{d}\mathcal{U}.$$

The following lemma and its proof can be found in (Balogh and Oraby 2025).

Lemma 11 *Consider a function $U \in C([0,\infty)\times\Omega, (0,\infty))$. Let $a(t)$ be a sequence such that*

$$\lim_{t\to\infty} \frac{a(t)}{t} = a > 0, \quad a.s.$$

and let b be a positive constant such that

$$\log(U(t)) \geq a(t) - b\int_0^t U(s)ds, \quad \textit{for all } t \geq 0, \quad a.s.$$

Then

$$\liminf_{t\to\infty} \frac{1}{t}\int_0^t U(s)\,ds \geq \frac{a}{b}, \quad a.s.$$

B.2 Inequalities

Let $U_i(t) > 0$ for $t \geq 0$ and $\omega_{i,i} = \sum_{j=1, j\neq i}^{N} \omega_{j,i}$ for $i = 1, 2, 3, \ldots, N$. Then

1.
$$\frac{1}{\zeta} - \frac{1+\eta\zeta}{\zeta^2}U_i \leq \frac{1}{(1+\eta U_i)(U_i+\zeta)} \leq \frac{1}{\zeta}.$$

2.
$$-\sum_{i=1}^{N}\omega_{i,i}U_i + \sum_{i=1}^{N}\sum_{j=1, j\neq i}^{N}\omega_{i,j}U_j = 0.$$

3.
$$\frac{\sigma_{\min}^2}{2N} \leq \frac{1}{2S^2}\sum_{i=1}^{N}\sigma_i^2 U_i^2.$$

Proof **Inequality 1:**
Since $U_i > 0$, $i = 1, 2, 3, \ldots, N$, it is straightforward that $\frac{1}{(1+\eta U_i)(U_i+\zeta)} \leq \frac{1}{\zeta}$. To show the other inequality, consider

$$\begin{aligned} H(U_i) &= \frac{1}{\zeta} - \frac{1+\eta\zeta}{\zeta^2}U_i - \frac{1}{(1+\eta U_i)(\zeta+U_i)} \\ &= \frac{\zeta(1+\eta U_i)(\zeta+U_i) - U_i(1+\eta\zeta)(1+\eta U_i)(\zeta+U_i) - \zeta^2}{\zeta^2(1+\eta U_i)(\zeta+U_i)} \\ &= \frac{-U_i^2 - \eta\zeta U_i^2 - \eta U_i^3 - \eta^2 U_i^2\zeta^2 - \eta^2 U_i^3\zeta}{\zeta^2(1+\eta U_i)(\zeta+U_i)}. \end{aligned}$$

Notice that every term in the numerator is non-positive, implying $H(U_i) \leq 0$. This observation leads to

$$\frac{1}{\zeta} - \frac{1+\eta\zeta}{\zeta^2}U_i \leq \frac{1}{(1+\eta U_i)(U_i+\zeta)}.$$

Equality 2: Note that,

$$\omega_{i,i} = \sum_{j=1, j\neq i}^{N}\omega_{j,i}.$$

We have,

$$-\sum_{i=1}^{N}\omega_{i,i}U_i = -\sum_{i=1}^{N}\left(\sum_{j=1,j\neq i}^{N}\omega_{j,i}\right)U_i = -\sum_{i=1}^{N}\sum_{j=1,j\neq i}^{N}\omega_{i,j}U_j.$$

Then,

$$-\sum_{i=1}^{N}\omega_{i,i}U_i + \sum_{i=1}^{N}\sum_{j=1,j\neq i}^{N}\omega_{i,j}U_j = -\sum_{i=1}^{N}\sum_{j=1,j\neq i}^{N}\omega_{i,j}U_j + \sum_{i=1}^{N}\sum_{j=1,j\neq i}^{N}\omega_{i,j}U_j = 0.$$

Inequality 3: It is clear that

$$\frac{\sigma_{\min}^2}{2S^2}\sum_{i=1}^{N}U_i^2 \leq \frac{1}{2S^2}\sum_{i=1}^{N}\sigma_i^2U_i^2.$$

From the Cauchy–Schwarz inequality, we have

$$\left(\sum_{i=1}^{N}U_i\right)^2 \leq N\sum_{i=1}^{N}U_i^2.$$

Note that $S = \sum_{i=1}^{N}U_i$, hence we have

$$\frac{\sigma_{\min}^2}{2N} \leq \frac{\sigma_{\min}^2}{2S^2}\sum_{i=1}^{N}U_i^2 \leq \frac{1}{2S^2}\sum_{i=1}^{N}\sigma_i^2U_i^2.$$

□

Appendix C: Calculation in theorem 6

Let $V : \mathbb{R}_+^N \to \mathbb{R}$ be defined as

$$V(U) = \log(S)$$

where $U = (U_1, U_2, \ldots, U_N)^T$ and $S = \sum_{i=1}^{N}U_i(t)$.

Itô's formula is given by

$$\mathrm{d}V = \frac{\partial V}{\partial U}\mathrm{d}U + \frac{1}{2}(\mathrm{d}U)^T\frac{\partial^2 V}{\partial U^2}(\mathrm{d}U).$$

We have

$$\frac{\partial V}{\partial U} = \left(\frac{1}{S}, \frac{1}{S}, \ldots, \frac{1}{S}\right),$$
$$\mathrm{d}U = (\mathrm{d}U_1, \mathrm{d}U_2, \ldots, \mathrm{d}U_N)^T,$$
$$\frac{\partial^2 V}{\partial^2 U} = \begin{bmatrix} -\frac{1}{S^2} & -\frac{1}{S^2} & \cdots & -\frac{1}{S^2} \\ -\frac{1}{S^2} & -\frac{1}{S^2} & \cdots & -\frac{1}{S^2} \\ . & . & \cdots & . \\ . & . & \cdots & . \\ . & . & \cdots & . \\ -\frac{1}{S^2} & -\frac{1}{S^2} & \cdots & -\frac{1}{S^2} \end{bmatrix}.$$

Using the above results in Itô's formula, we get

$$\mathrm{d}V = \frac{1}{S}\sum_{i=1}^{N} \mathrm{d}U_i + \frac{1}{2}\left(-\frac{1}{S^2}\right)\left(\sum_{i=1}^{N} \mathrm{d}U_i\right)^2.$$

Substituting $\mathrm{d}U_i$ into $\mathrm{d}V$. The first term becomes

$$\frac{1}{S}\sum_{i=1}^{N} \mathrm{d}U_i = \frac{1}{S}\sum_{i=1}^{N} U_i \left[\frac{1}{(1+\eta U_i)(U_i+\zeta)} - 1 - \omega_{i,i} + \sum_{j\neq i}^{N} \omega_{i,j}\frac{U_j}{U_i}\right]\mathrm{d}t + \frac{1}{S}\sum_{i=1}^{N} \sigma_i U_i \,\mathrm{d}W_i(t).$$

We have

$$\left(\sum_{i=1}^{N} \mathrm{d}U_i\right)^2 = \left(\sum_{i=1}^{N} U_i \left[\frac{1}{(1+\eta U_i)(U_i+\zeta)} - 1 - \omega_{i,i} + \sum_{j\neq i}^{N} \omega_{i,j}\frac{U_j}{U_i}\right]\mathrm{d}t + \sum_{i=1}^{N} \sigma_i U_i \,\mathrm{d}W_i(t)\right)^2.$$

By using the following Itô rules

$$\mathrm{d}t\,\mathrm{d}t = 0, \quad \mathrm{d}W_i\,\mathrm{d}t = 0, \quad \mathrm{d}W_i\,\mathrm{d}W_i = \mathrm{d}t, \quad \mathrm{d}W_i\,\mathrm{d}W_j = 0 \quad \text{for } i \neq j.$$

We get,

$$\left(\sum_{i=1}^{N} \mathrm{d}U_i\right)^2 = \sum_{i=1}^{N} \sigma_i^2 U_i^2 \,\mathrm{d}t.$$

Combining all the terms, the final expression for $\mathrm{d}V$ is

$$\mathrm{d}V = \frac{1}{S}\sum_{i=1}^{N} U_i \left[\frac{1}{(1+\eta U_i)(U_i+\zeta)} - 1 - \omega_{i,i} + \sum_{j\neq i}^{N} \omega_{i,j}\frac{U_j}{U_i}\right]\mathrm{d}t$$

$$+\frac{1}{S}\sum_{i=1}^{N}\sigma_i U_i\,\mathrm{d}W_i-\frac{1}{2S^2}\sum_{i=1}^{N}\sigma_i^2 U_i^2\,\mathrm{d}t.$$

Appendix D: Analytical solution to deterministic model

Here, we derive the formula to find the toxic protein concentration at a given time using the scalar deterministic model

$$\frac{\mathrm{d}U}{\mathrm{d}t}=U\left(\frac{1}{(1+\eta U)(U+\zeta)}-1\right).$$

Solving above first order differential equation we obtain

$$C_1\ln U+C_2\ln|U-U^+|+C_3\ln(U-U^-)=t+K, \tag{D3}$$

for $U\neq 0$ and $U\neq U^+$. Here K is an arbitrary integration constant and

$$\begin{aligned}
U^+&=\frac{-(1+\eta\zeta)+\sqrt{(1+\eta\zeta)^2-4\eta(\zeta-1)}}{2\eta},\\
U^-&=\frac{-(1+\eta\zeta)-\sqrt{(1+\eta\zeta)^2-4\eta(\zeta-1)}}{2\eta},\\
C_1&=\frac{\zeta}{(U^+)(U^-)},\\
C_2&=\frac{(1+\eta U^+)(U^++\zeta)}{U^+(U^+-U^-)},\\
C_3&=\frac{(1+\eta U^+)(U^++\zeta)}{U^-(U^+-U^-)}.
\end{aligned}$$

Define $F:\mathbb{R}^+\to\mathbb{R}^+$ by $F(U)=C_1\ln U+C_2\ln|U-U^+|+C_3\ln(U-U^-)$. For a given $0<U(0)<U^+$ or $U^+<U(0)$, one can compute toxic protein concentration $U(t)$ at any time t using any suitable numerical scheme for the transcendental equation $F(U)=t+K$, where $K=C_1\ln(U(0))+C_2\ln|U(0)-U^+|+C_3\ln(U(0)-U^-)$.

Appendix E: Derivation of the model

To nondimensionalize equations (1)–(2), we use the transformations

$$t=\bar{t}\,t^*,\quad X(t)=\overline{X}\,X^*(t^*),\quad Y(t)=\overline{Y}\,Y^*(t^*),$$

where the overbars indicate characteristic scales, and the variables with an asterisk are dimensionless. After using $\bar{t}=\frac{1}{\beta}$, $\overline{X}=\frac{\beta}{\gamma}$, $\overline{Y}=A\bar{t}$, simplifying and omitting the

overbars and asterisks, we get

$$\begin{aligned} \mathrm{d}X &= \left(\frac{\frac{A\gamma}{\beta^2}}{1+\eta Y(t-\tau)} - \frac{A\gamma}{\beta^2} XY - \frac{\alpha}{\beta} X \right) \mathrm{d}t + \rho_X X \mathrm{d}W_X(t), \\ \mathrm{d}Y &= (XY - Y)\mathrm{d}t + \rho_Y Y \mathrm{d}W_Y(t), \end{aligned}$$

with initial conditions $X(0) = \hat{X}$ and $Y(t) = \hat{Y}(t),\ t \in [-\tau, 0]$. Where

$$\eta = \frac{\overline{Y}}{Y_c},\ \tau = t_d\beta,\ \rho_X = \sigma\sqrt{\alpha},\ \text{and}\ \rho_Y = \sigma\sqrt{\beta}.$$

Estimation of ρ_X and ρ_Y are discussed in Appendix F. Upon considering biologically relevant parameter values, $\epsilon = \frac{\beta}{\alpha}$ serves as an asymptotic scale, while $R_0 = \frac{A\gamma}{\alpha\beta} = O(1)$ and $\eta = O(1)$. These quantities appear to be $O(1)$ in clinical data (see Table 8). Consequently, we obtain

$$\mathrm{d}X^\varepsilon = \frac{1}{\varepsilon}\left(\frac{R_0}{1+\eta Y^\varepsilon(t-\tau)} - R_0 X^\varepsilon Y^\varepsilon - X^\varepsilon \right) \mathrm{d}t + \frac{\sigma}{\sqrt{\varepsilon}} X^\varepsilon \mathrm{d}W_X(t), \tag{E4}$$

$$\mathrm{d}Y^\varepsilon = (X^\varepsilon Y^\varepsilon - Y^\varepsilon)\mathrm{d}t + \sigma Y^\varepsilon \mathrm{d}W_Y(t). \tag{E5}$$

Note that $Y^\varepsilon(t-\tau) = \hat{Y}(t-\tau)$ for $t \in [0, \tau]$ is a nonnegative continuous function. Following the literature (Liu et al. 2020) for the time interval $[0, \tau]$, Y^ε converges to Y, that is for some $p > 0$,

$$\lim_{\epsilon \to 0} \mathbb{E}\left(\sup_{t\in[0,\tau]} |Y^\varepsilon(t) - Y(t)|^p \right) = 0,$$

where Y is the solution of the corresponding averaged equation

$$\mathrm{d}Y = b(t, Y)\mathrm{d}t + \sigma Y \mathrm{d}W_Y(t),\ t \in [0, \tau].$$

Here $b(t, y) = y\int_{\mathbb{R}}(X-1)\mu^{t,y}(\mathrm{d}X) = y\left(\mathbb{E}_{\mu^{t,y}}(X) - 1\right),\ t \in [0, \tau]$ and $\mu^{t,y}$ denotes the invariant measure for the transition semigroup of the following frozen equation

$$\mathrm{d}X(s) = \left(\frac{R_0}{1+\eta y(t-\tau)} - (R_0 y(t) + 1)X(s) \right) \mathrm{d}s + \sigma X(s)\mathrm{d}W_X(s),\ s \in [0, \tau],$$

with $X(0) = \hat{X}$. Therefore, model for toxic protein dynamic is

$$\mathrm{d}Y = Y\left(\frac{R_0}{(1+\eta Y(t-\tau))(R_0 Y(t) + 1)} - 1 \right) \mathrm{d}t + \sigma Y \mathrm{d}W_Y(t),\ Y(t-\tau) = \hat{Y}(t), \tag{E6}$$

for $t \in [0, \tau]$. Since $\mathbb{E}_{\mu^{t,y}}(X) = \frac{R_0}{(1+\eta Y(t-\tau))(R_0 Y(t)+1)}$ (Nafidi et al. 2019). Shifting equations (E4)–(E5) from the interval $[0, \tau]$ to $[\tau, 2\tau]$, together with the corresponding initial conditions, and then following the approach in Liu et al. (2020) for the time interval $[\tau, 2\tau]$, we obtain the model for toxic protein dynamics (equation (E6)) on the time interval $[0, 2\tau]$. Similarly, by employing a ladder argument, equation (E6) can be derived for any time interval $[0, T]$ with $0 < \tau \leq T$.

To avoid notational ambiguity in the subsequent analysis, we set

$$Y = U, \quad \zeta = \frac{1}{R_0}, \quad \text{and} \quad \mathrm{d}W_Y(t) = \mathrm{d}W(t).$$

Consequently, the governing equation (E6) can be rewritten as

$$\begin{aligned} \mathrm{d}U &= \left(\frac{U}{(1+\eta U(t-\tau))(U+\zeta)} - U \right) \mathrm{d}t + \sigma U \, \mathrm{d}W(t), \\ U(t-\tau) &= \phi(t), \end{aligned} \tag{E7}$$

for $t \geq 0$.

Similarly, for the connectome model (6)–(7), we apply the transformation

$$t = \bar{t}\, t^*, \quad X_i(t) = \overline{X}\, X_i^*(t^*), \quad Y_i(t) = \overline{Y}\, Y_i^*(t^*), \quad i = 1, 2, 3, \ldots, N,$$

where the overbars denote characteristic scales and the variables with an asterisk are dimensionless. Using

$$\bar{t} = \frac{1}{\beta}, \quad \overline{X} = \frac{\beta}{\gamma}, \quad \overline{Y} = A\bar{t},$$

and simplifying and omitting the overbars and asterisks, we obtain

$$\begin{aligned} \mathrm{d}X_i &= \left(\frac{\frac{A\gamma}{\beta^2}}{1+\eta Y_i(t-\tau)} - \frac{A\gamma}{\beta^2} X_i Y_i - \frac{\alpha}{\beta} X_i \right) \mathrm{d}t + \sigma_{X,i} X_i \mathrm{d}W_{X,i}(t), \\ \mathrm{d}Y_i &= \left(\sum_{j=1, j\neq i}^{N} \omega_{i,j} Y_j - \omega_{i,i} Y_i + X_i Y_i - Y_i \right) \mathrm{d}t + \sigma_{Y,i} Y_i \, \mathrm{d}W_{Y,i}(t), \end{aligned}$$

for $i = 1, 2, 3, \ldots, N$, where

$$\eta = \frac{\overline{Y}}{Y_c}, \ \tau = t_d \beta, \ \rho_{X,i} = \sigma_i \sqrt{\alpha}, \ \rho_{Y,i} = \sigma_i \sqrt{\beta}, \text{ and } \omega_{i,j} = r \frac{L_{i,j}}{\beta},$$

for $i, j = 1, 2, 3, \ldots, N$. We take $\epsilon = \frac{\beta}{\alpha}$ as an asymptotic scale, while $R_0 = \frac{A\gamma}{\alpha\beta} = O(1)$, $w_{i,j} = O(1)$, and $\eta = O(1)$. These quantities are observed to be of order one in clinical data (see Table 8). Consequently, the system reduces to

$$\mathrm{d}X_i^\varepsilon = \frac{1}{\varepsilon} \left(\frac{R_0}{1+\eta Y_i^\varepsilon(t-\tau)} - R_0 X_i^\varepsilon Y_i^\varepsilon - X_i^\varepsilon \right) \mathrm{d}t + \frac{\sigma_i}{\sqrt{\varepsilon}} X_i^\varepsilon \mathrm{d}W_{X,i}(t),$$

$$\mathrm{d}Y_i^{\varepsilon} = \left(\sum_{j=1, j\neq i}^{N} \omega_{i,j} Y_j^{\varepsilon} - \omega_{i,i} Y_i^{\varepsilon} + X_i^{\varepsilon} Y_i^{\varepsilon} - Y_i^{\varepsilon} \right) \mathrm{d}t + \sigma_i Y_i^{\varepsilon} \, \mathrm{d}W_{Y,i}(t).$$

Using same arguments as discussed in the scalar case, we obtain a reduced model that captures the dynamics of the toxic protein in the connectome:

$$\begin{aligned} \mathrm{d}U_i = &\left(\frac{U_i}{(1+\eta U_i(t-\tau))(U_i+\zeta)} - U_i - \omega_{i,i} U_i + \sum_{j=1, j\neq i}^{N} \omega_{i,j} U_j \right) \mathrm{d}t \\ &+ \sigma_i U_i \, \mathrm{d}W_i(t), \, U_i(t-\tau) = \phi_i(t), \end{aligned} \tag{E8}$$

for $i = 1, 2, \ldots, N$ and $t \geq 0$.

Appendix F: Parameter values

Parameters ρ_X, ρ_Y, etc.

We focus upon clearance where Geometric Brownian Motion can be used as a simple model to account for fluctuations in clearance rate (Ditlevsen and Samson 2012), i.e., the protein concentration P evolves with time t according to

$$\mathrm{d}P = -\nu P \mathrm{d}t + \varsigma P \mathrm{d}W,$$

where ν is a clearance rate, ς is a volatility, and W is a Brownian motion. We propose there is an intrinsic relationship

$$\varsigma = V(\nu),$$

for an unknown function V. By dimensional analysis, the units of ς are $\mathrm{T}^{-1/2}$ and the units of ν are T^{-1} (T is time) and thus it is also true that

$$\varpi = v(\nu),$$

where $\varpi = \frac{\varsigma}{\sqrt{\nu}}$ is dimensionless and $V = \sqrt{\nu} v$. Since the left is dimensionless (thus invariant under changes of units) and the right, v, depends on a dimensional variable, we conclude that $v(\nu)$ and ϖ are constants by a Buckingham Pi argument (see Bluman and Kumei (1989)).

Having $\varsigma = \varpi \sqrt{\nu}$, we sought experimental data that directly measure the clearance of proteins in the brain. In McIntee et al. (2016), the authors measured the clearance of Aβ monomers and oligomers in the brains of mice. Both Aβ and prions have similar spreading and templating mechansisms in pathological forms (Wang et al. 2025), and there is overlap in their clearance mechanisms, such as lysosomal degradation, the ubiquitin-proteasome-system, and phagocytosis (Ullah and Lee 2023; Goold et al. 2015; Aguzzi et al. 2017). Based on their similarities, we used the Aβ clearance data as a proxy to establish the clearance-volatility relationship.

We separately fit for ν and ς using the brain clearance data of Aβ monomers and Aβ oligomers (McIntee et al. 2016) separately. We used the maximum likelihood estimators (Nkemnole and Abass 2019) to find values ν and ς, the Fisher information (Yuan et al. 2014) to estimate uncertainties, and applied the delta method (Ver Hoef 2012) to estimate $\varpi = \frac{\varsigma}{\sqrt{\nu}}$ with a standard error. For monomers, we found $\varpi = 0.55 \pm 0.30$ and for oligomers we found 0.42 ± 0.22 (where the $\pm$ denote standard error). The two estimates agree well and we averaged them to estimate $\varpi = 0.5 \pm 0.2$ using quadrature for the errors.

Regarding our best estimates for clinically relevant parameters, we adopt $\rho_X = \varpi\sqrt{\alpha}$ and $\rho_Y = \varpi\sqrt{\beta}$ with $\varpi = 0.5$ (with the same relationship applying in all brain regions). For a more general theory, however, we assume that there is an $O(1)$ constant σ describing the ratio of volatility to the square root of clearance (and likewise with the σ_i for each brain region i).

Parameter Y_c

We note that, in the terminal stage of scrapie, the concentration of toxic protein is approximately 100 µg per gram of brain tissue (Beekes et al. 1996). Since the density of brain tissue is approximately $1\,\mathrm{g\,cm^{-3}}$ (Barber et al. 1970), this corresponds to a volumetric concentration of about $1 \times 10^{-4}\,\mathrm{g\,cm^{-3}}$. Assuming that the terminal-stage concentration represents the steady state level of toxicity (Y_∞), we therefore set

$$Y_\infty \approx 1 \times 10^{-4}\,\mathrm{g\,cm^{-3}}.$$

We estimate the parameter Y_c with

$$\frac{\mathrm{d}Y_\infty}{\mathrm{d}t} = \left(\frac{\gamma A Y_\infty}{(1 + \frac{Y_\infty}{Y_c})(\gamma Y_\infty + \alpha)} - \beta Y_\infty \right) = 0.$$

This implies that

$$Y_c = \frac{Y_\infty}{\frac{\gamma A}{\beta(\gamma Y_\infty + \alpha)} - 1} \approx 3 \times 10^{-4}\,\mathrm{g\,cm^{-3}}. \tag{F9}$$

Parameter r.

We estimate the parameter r by fitting the deterministic network-based model

$$\mathrm{d}X_i = \left(\frac{A}{1 + \frac{Y_i(t - t_d)}{Y_c}} - \gamma X_i Y_i - \alpha X_i \right) \mathrm{d}t, \tag{F10}$$

$$\mathrm{d}Y_i = \left(r \sum_{j=1, j\neq i}^{N} L_{i,j} Y_j - r L_{i,i} Y_i + \gamma X_i Y_i - \beta Y_i \right) \mathrm{d}t, \tag{F11}$$

for $i = 1, 2, 3 \ldots 83$. Additional details regarding node indices and their corresponding regions are provided in (Fornari et al. 2020) and its supplementary material. We further assume that the state variables X_i and Y_i represent the average concentrations within each region i, and that all regions have equal volume. Under these assumptions, volume

corrections are not required when modeling protein transport between regions. To fit the parameter r, we used the experimental results reported in (Beekes et al. 1996). In this experiment, hamsters were infected orally by feeding each animal 10 mg of homogenized brain tissue obtained from a hamster in the terminal stage of scrapie. Brain samples (approximately 1 g of tissue) were collected from the hamsters at the following days post-infection (p.i.): 77, 86, 91, 95, 100, 105, 109, 114, 119, 123, 127, and 133. The authors reported that toxic protein was first detected in the brain at 100 days p.i., and was subsequently observed at all later time points. The mean concentration of toxic protein at 100 days p.i. and 133 days p.i. was reported to be approximately 1.58×10^{-7} g cm^{-3} and 1×10^{-5} g cm^{-3}, respectively.

The study in (Beekes et al. 1998) investigated the sequential appearance of toxic protein in the brains of orally infected hamsters and reported that the first target region is the dorsal motor nucleus of the vagus nerve, which is part of the brain stem. Accordingly, we choose the brain stem as the initial seeding region. The initial concentration in the brain stem is determined from

$$\frac{1}{83}\sum_{i=1}^{83}\tilde{Y}_i = 1.58 \times 10^{-7}\, g\,\mathrm{cm}^{-3},$$

where $\tilde{Y}_i$ denotes the experimentally measured toxic protein concentration in brain region i, and the summation represents the mean concentration over the brain. At 100 days p.i., we assume that $\tilde{Y}_i = 0$ for all nodes that do not belong to the brain stem (the brain stem being node 83). This implies

$$\tilde{Y}_i = \begin{cases} 0, & \text{if } i = 1, 2, \ldots, 82, \\ 1 \times 10^{-5} g\,\mathrm{cm}^{-3}, & \text{if } i = 83. \end{cases}$$

We choose initial conditions $Y_i(0) = \tilde{Y}_i$ for $i = 1, 2, \ldots, 83$ and $X_i = \frac{A}{\alpha}$ for $i = 1, 2, \ldots, 83$, corresponding to the steady state in the absence of toxic protein. We fit the r so that $\frac{1}{83}\sum_{i=1}^{83} Y_i(\hat{T}) = 10^{-5}\,\mathrm{g\,cm}^{-3}$ at $\hat{T} = 33$ days (133 days -100 days). We choose $r = 5 \times 10^{-3}\,\mathrm{cm\,day}^{-1}$, as this value allows the mean toxic concentration to reach $1 \times 10^{-5}\,\mathrm{g\,cm}^{-3}$ at 33 days, as shown in Fig. 13. However, accounting for approximation errors in the extracted experimental data, we introduce a tolerance window of 33 days ($\pm 5\%$) and $1 \times 10^{-5}\,\mathrm{g\,cm}^{-3}$ ($\pm 5\%$) for the mean toxic concentration. We find the approximate range for r to enter the window is $\underline{r} = 2 \times 10^{-3}$ cm day^{-1} to $\overline{r} = 1$ cm day^{-1}. We acknowledge that the estimation of r relies on non-human data, which constitutes a limitation of the present study and will be addressed in future work.

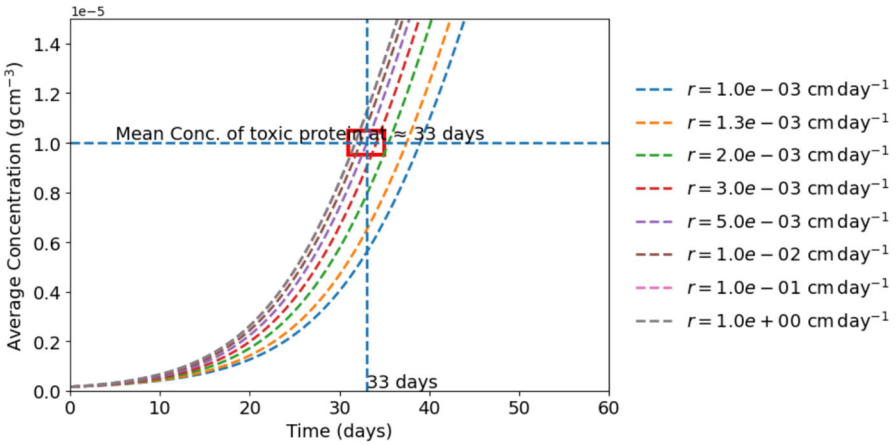

Fig. 13 Model-based estimation of the parameter r using experimental prion concentration data (Beekes et al. 1996, 1998). The curves show the predicted average toxic prion concentration for several values of r. The rectangular box denotes the tolerance window of 33 days (±5%) and 1×10^{-5} g cm^{-3} (±5%) for the mean toxic concentration

Table 8 Estimated values for clinical model

Parameter	Value
$\varepsilon = \frac{\beta}{\alpha}$	6×10^{-3}
$R_0 = \frac{A\gamma}{\alpha\beta}$	5
$\zeta = \frac{\alpha\beta}{A\gamma}$	0.2
$\eta = \frac{A}{\beta Y_c}$	0.6
$\tau = t_d\beta$	2×10^{-2}
$\sigma_i, i = 1, 2, \ldots, N$	0.5
$\max_{i,j}\{\omega_{i,j}\}$	2×10^{1}

Appendix G: Oscillatory behavior in connectome model

Due to the complexity of the system and the extensive computational effort required, a detailed Hopf bifurcation analysis for the system is deferred to future work. However, our numerical simulations indicate the emergence of oscillatory behavior in the system for certain values of the time delay parameter. This observation suggests the possibility of a delay-induced transition to periodic dynamics, which is an important phenomenon in the study of time-delayed differential equations.

To explore this effect, we consider a simplified model with three brain regions, denoted by R_1, R_2, and R_3, each initially assigned a toxic concentration: $U_1(0) = 0.1$, $U_2(0) = 0.3$, and $U_3(0) = 0.5$. The noise intensity is assumed to be the same in all regions, i.e., $\sigma_1 = \sigma_2 = \sigma_3 = \sigma$. The interactions between these regions are

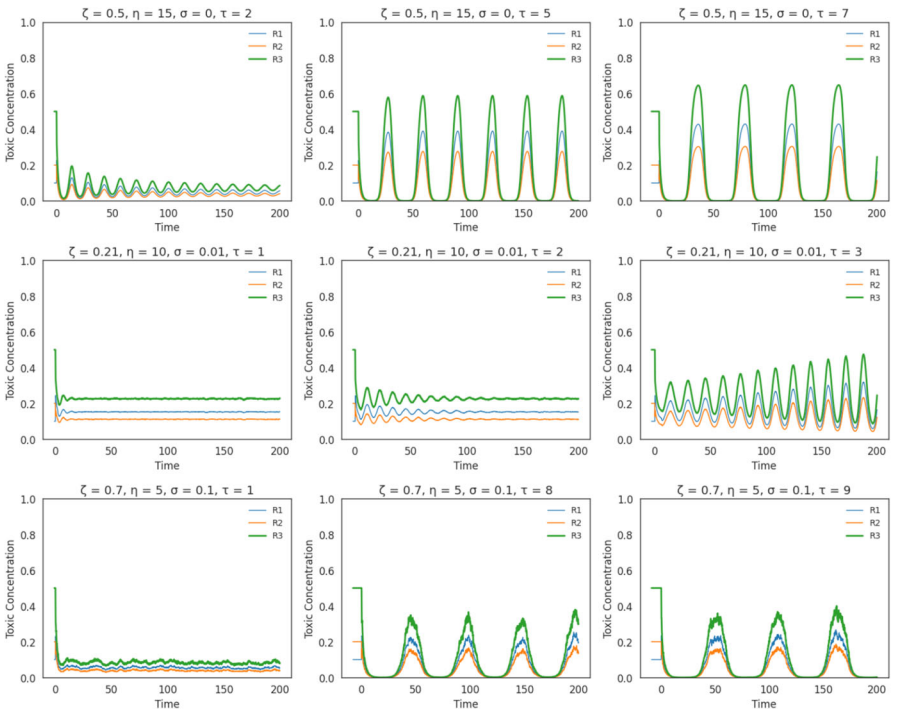

Fig. 14 Numerical solution of equation (49) showing existence of Hopf bifurcation in the connectome model

represented by an arbitrary connectome matrix

$$\omega = \begin{bmatrix} -6 & 2 & 3 \\ 4 & -8 & 1 \\ 2 & 6 & -4 \end{bmatrix}$$

To investigate the impact of time delay on system dynamics, we numerically solve equation (49) using Milstein's method and analyze the resulting time series. Fig. 14 presents the time evolution of toxic concentration in the three regions for different values of the time delay parameter τ. Our findings reveal that for small time delays, oscillations in the system are damped out. However, as the time delay increases beyond a critical threshold, sustained periodic oscillations emerge, indicating a transition to a stable limit cycle.

When the biological processing time required to activate the UPR is increased from 0 to 77 days, with $\rho_{Y,i} = 0\ \mathrm{s}^{-\frac{1}{2}}$, $i = 1, 2, \ldots, 83$, $\beta = 3 \times 10^{-8}\ \mathrm{s}^{-1}$, $\alpha = 1.7 \times 10^{-3}\ \mathrm{s}^{-1}$, and all other parameters remaining the same as in Table 5, the toxic protein concentration exhibits oscillatory behavior in 83 brain regions, as illustrated in Fig. 15. In contrast, for the clinical parameter values listed in Table 5, using the biological connectome and varying the time delay, oscillatory behavior was not observed, as shown in Fig. 16.

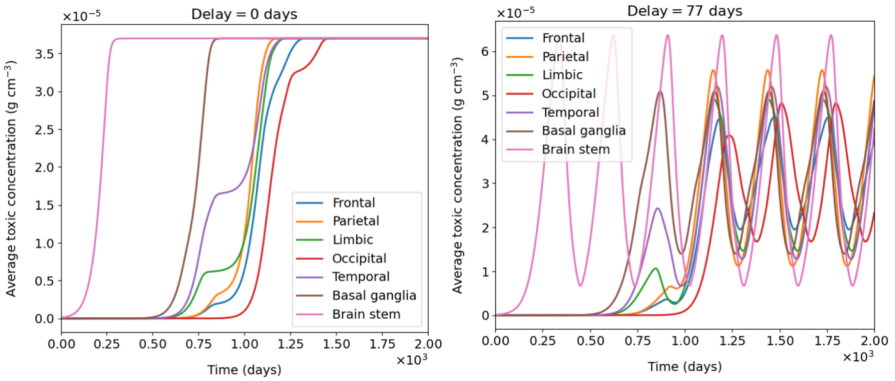

Fig. 15 The average toxic protein concentration in the brain connectome exhibits oscillations at a time delay of 77 days for, $\rho_{Y,i} = 0\ \mathrm{s}^{-\frac{1}{2}}$, $i = 1, 2, \ldots, 83$, $\beta = 3 \times 10^{-8}\ \mathrm{s}^{-1}$ and $\alpha = 1.7 \times 10^{-3}\ \mathrm{s}^{-1}$. All other parameters are listed in Table 5

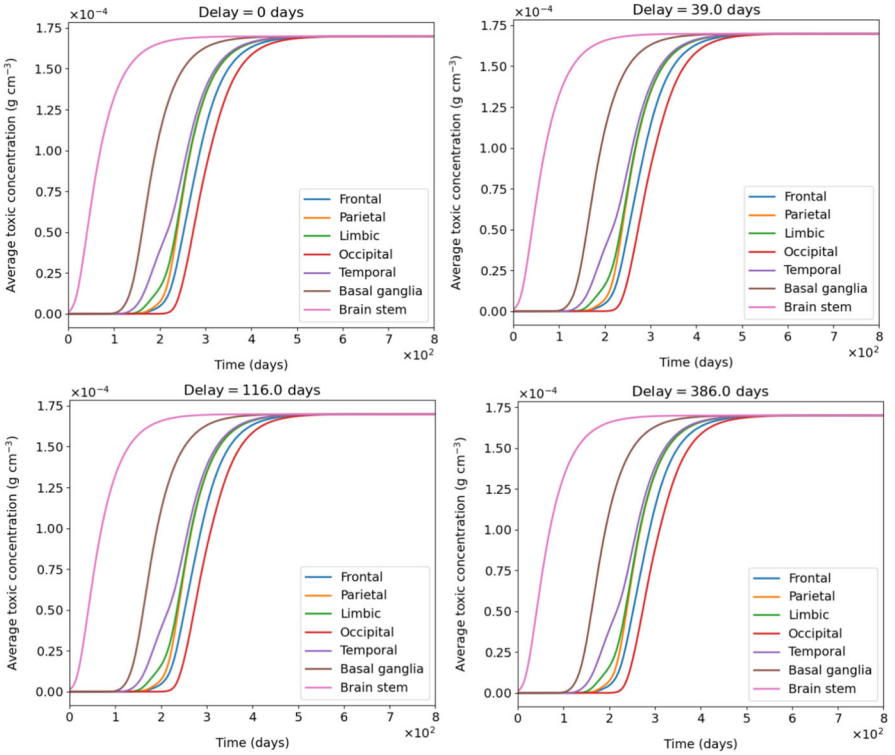

Fig. 16 The average toxic protein concentration in the brain connectome shows no oscillations for large time delays. All other parameters are listed in Table 5

A systematic investigation of the uncertainty in these parameters using Hopf bifurcation analysis for the connectome model is left for future work. These simulations suggest a start–stop mechanism of the UPR under long biological processing times, which may drive neurons into an oscillatory stress state depending on their local environment.

Acknowledgements This project has received support from NSF Award DMS #2316952 and NSF Award DMS #2150478. This project has received support from Agence Nationale de la Recherche PrionDiff Project-ANR-21-CE15-0011. The authors would like to thank Erwin Suazo for supporting students in this work.

Data availability We used brain connectome data from the Budapest Reference Connectome v3.0 (Szalkai et al. 2015), and the cleaned and processed data are available upon request.

Declarations

Conflicts of interest The authors declare that there is no conflict of interest.

Open Access This article is licensed under a Creative Commons Attribution-NonCommercial-NoDerivatives 4.0 International License, which permits any non-commercial use, sharing, distribution and reproduction in any medium or format, as long as you give appropriate credit to the original author(s) and the source, provide a link to the Creative Commons licence, and indicate if you modified the licensed material. You do not have permission under this licence to share adapted material derived from this article or parts of it. The images or other third party material in this article are included in the article's Creative Commons licence, unless indicated otherwise in a credit line to the material. If material is not included in the article's Creative Commons licence and your intended use is not permitted by statutory regulation or exceeds the permitted use, you will need to obtain permission directly from the copyright holder. To view a copy of this licence, visit http://creativecommons.org/licenses/by-nc-nd/4.0/.

References

Akhtar A, Andleeb A, Waris TS, Bazzar M, Moradi A-R, Awan NR, Yar M (2021) Neurodegenerative diseases and effective drug delivery: A review of challenges and novel therapeutics. J Control Release 330:1152–1167

Adimy M, Babin L, Pujo-Menjouet L (2022) Neuron scale modeling of prion production with the unfolded protein response. SIAM J Appl Dyn Syst 21(4):2487–2517

Applebaum D (2009) Lévy Processes and Stochastic Calculus. Cambridge University Press, United Kingdom

Assembly F (2002) An analytical solution to the kinetics of breakable. Geology 30:251

Aguzzi A, Zhu C et al (2017) Microglia in prion diseases. J Clin Investig 127(9):3230–3239

Atkinson CJ, Zhang K, Munn AL, Wiegmans A, Wei MQ (2016) Prion protein scrapie and the normal cellular prion protein. Prion 10(1):63–82

Beekes M, Baldauf E, Diringer H (1996) Sequential appearance and accumulation of pathognomonic markers in the central nervous system of hamsters orally infected with scrapie. J Gen Virol 77(8):1925–1934

Barber TW, Brockway JA, Higgins LS (1970) The density of tissues in and about the head. Acta Neurol Scand 46(1):85–92

Bertsch M, Franchi B, Tesi MC, Tosin A (2017) Microscopic and macroscopic models for the onset and progression of Alzheimer's disease. J Phys A: Math Theor 50(41):414003

Bertsch M, Franchi B, Tesi MC, Tora V (2023) The role of a β and tau proteins in Alzheimer's disease: A mathematical model on graphs. J Math Biol 87(3):49

Bluman GW, Kumei S (1989) Symmetries and Differential Equations, vol 81. Springer, New York

Boregowda G, Lindstrom MR (2025) Existence and stability theory of a neurologically inspired parabolic pde model with a nonlinear time-delayed boundary condition. International Journal of Bifurcation and Chaos 35(15):2550170

Beekes M, McBride PA, Baldauf E (1998) Cerebral targeting indicates vagal spread of infection in hamsters fed with scrapie. J Gen Virol 79(3):601–607

Balogh A, Oraby T (2025) Stochastic games of parental vaccination decision making and bounded rationality. Math Biosci Eng 22(2):355–388

Çalış Y, Demirci A, Özemir C (2022) Hopf bifurcation of a financial dynamical system with delay. Math Comput Simul 201:343–361

Chung TJ (2002) Computational Fluid Dynamics. Cambridge University Press, United Kingdom

Davie CA (2008) A review of Parkinson's disease. Br Med Bull 86(1):109–127

Desplats P, Lee H-J, Bae E-J, Patrick C, Rockenstein E, Crews L, Spencer B, Masliah E, Lee S-J (2009) Inclusion formation and neuronal cell death through neuron-to-neuron transmission of α-synuclein. Proc Natl Acad Sci 106(31):13010–13015

DebBurman SK, Raymond GJ, Caughey B, Lindquist S (1997) Chaperone-supervised conversion of prion protein to its protease-resistant form. Proc Natl Acad Sci 94(25):13938–13943

Ditlevsen S, Samson A (2012) Introduction to stochastic models in biology. In: Stochastic Biomathematical Models: with Applications to Neuronal Modeling, pp. 3–35. Springer, Berlin

Fornari S, Schäfer A, Jucker M, Goriely A, Kuhl E (2019) Prion-like spreading of Alzheimer's disease within the brain's connectome. J R Soc Interface 16(159):20190356

Fornari S, Schäfer A, Kuhl E, Goriely A (2020) Spatially-extended nucleation-aggregation-fragmentation models for the dynamics of prion-like neurodegenerative protein-spreading in the brain and its connectome. J Theor Biol 486:110102

Geschwind MD (2015) Prion diseases. Continuum Lifelong Learning in Neurology 21(6):1612–1638

Goold R, McKinnon C, Tabrizi SJ (2015) Prion degradation pathways: Potential for therapeutic intervention. Mol Cell Neurosci 66:12–20

Goedert M, Spillantini MG (2006) A century of Alzheimer's disease. Science 314(5800):777–781

Genereux JC, Wiseman RL (2015) Regulating extracellular proteostasis capacity through the unfolded protein response. Prion 9(1):10–21

Hao W, Friedman A (2016) Mathematical model on Alzheimer's disease. BMC Syst Biol 10(1):1–18

Jack CR Jr, Bennett DA, Blennow K, Carrillo MC, Dunn B, Haeberlein SB, Holtzman DM, Jagust W, Jessen F, Karlawish J et al (2018) Nia-aa research framework: toward a biological definition of Alzheimer's disease. Alzheimer's & Dementia 14(4):535–562

Jiang D, Yu J, Ji C, Shi N (2011) Asymptotic behavior of global positive solution to a stochastic sir model. Math Comput Model 54(1–2):221–232

Kiaei M (2013) New hopes and challenges for treatment of neurodegenerative disorders: Great opportunities for young neuroscientists. Basic and Clinical Neuroscience 4(1):3

Lindstrom MR, Chavez MB, Gross-Sable EA, Hayden EY, Teplow DB (2021) From reaction kinetics to dementia: A simple dimer model of Alzheimer's disease etiology. PLoS Comput Biol 17(7):1009114

Livezey M, Huang R, Hergenrother PJ, Shapiro DJ (2018) Strong and sustained activation of the anticipatory unfolded protein response induces necrotic cell death. Cell Death & Differentiation 25(10):1796–1807

Liu W, Röckner M, Sun X, Xie Y (2020) Averaging principle for slow-fast stochastic differential equations with time dependent locally lipschitz coefficients. J Differential Equations 268(6):2910–2948

Mao X (2007) Stochastic Differential Equations and Applications. Elsevier, United Kingdom

Miller EM, Chan TCD, Montes-Matamoros C, Sharif O, Pujo-Menjouet L, Lindstrom MR (2024) Oscillations in neuronal activity: a neuron-centered spatiotemporal model of the unfolded protein response in prion diseases. Bull Math Biol 86(7):82

McIntee FL, Giannoni P, Blais S, Sommer G, Neubert TA, Rostagno A, Ghiso J (2016) In vivo differential brain clearance and catabolism of monomeric and oligomeric alzheimer's aβ protein. Frontiers in Aging Neuroscience 8:223

Moreno JA, Halliday M, Molloy C, Radford H, Verity N, Axten JM, Ortori CA, Willis AE, Fischer PM, Barrett DA et al (2013) Oral treatment targeting the unfolded protein response prevents neurodegeneration and clinical disease in prion-infected mice. Science Translational Medicine 5(206):206–138206138

Mil'shtein GN (1979) A method of second-order accuracy integration of stochastic differential equations. Theory of Probability & Its Applications 23(2):396–401

Moreno JA, Radford H, Peretti D, Steinert JR, Verity N, Martin MG, Halliday M, Morgan J, Dinsdale D, Ortori CA et al (2012) Sustained translational repression by eif2α-p mediates prion neurodegeneration. Nature 485(7399):507–511

Nkemnole B, Abass O (2019) Estimation of geometric brownian motion model with at-distribution-based particle filter. Journal of Economic and Financial Sciences 12(1):1–9

Nafidi A, Moutabir G, Gutiérrez-Sánchez R (2019) Stochastic brennan-schwartz diffusion process: Statistical computation and application. Mathematics 7(11):1062

Ono K, Condron MM, Teplow DB (2009) Structure-neurotoxicity relationships of amyloid β-protein oligomers. Proc Natl Acad Sci 106(35):14745–14750

Pao CV (2012) Nonlinear Parabolic and Elliptic Equations. Springer, New York

Peña J, Harris E (2011) Dengue virus modulates the unfolded protein response in a time-dependent manner. J Biol Chem 286(16):14226–14236

Prusiner SB (1989) Creutzfeldt-jakob disease and scrapie prions. Alzheimer Disease & Associated Disorders 3(1):52–78

Raj A, Kuceyeski A, Weiner M (2012) A network diffusion model of disease progression in dementia. Neuron 73(6):1204–1215

Rangel A, Race B, Striebel J, Chesebro B (2013) Non-amyloid and amyloid prion protein deposits in prion-infected mice differ in blockage of interstitial brain fluid. Neuropathol Appl Neurobiol 39(3):217–230

Ruan S, Wei J (2003) On the zeros of transcendental functions with applications to stability of delay differential equations with two delays. Dynamics of Continuous Discrete and Impulsive Systems Series A 10:863–874

Saqlain M, Alam M, Rönnegård L, Westin J (2020) Investigating stochastic differential equations modelling for levodopa infusion in patients with Parkinson's disease. Eur J Drug Metab Pharmacokinet 45:41–49

Shafiq M, Da Vela S, Amin L, Younas N, Harris DA, Zerr I, Altmeppen HC, Svergun D, Glatzel M (1869) Glatzel, M (2022) The prion protein and its ligands: Insights into structure-function relationships. Biochimica et Biophysica Acta (BBA)-Molecular Cell Research 6:119240

Selkoe DJ (2003) Folding proteins in fatal ways. Nature 426(6968):900–904

Szalkai B, Kerepesi C, Varga B, Grolmusz V (2015) The budapest reference connectome server v2. 0. Neurosci Lett 595:60–62

Shaheen H, Pal S, Melnik R (2023) Astrocytic clearance and fragmentation of toxic proteins in Alzheimer's disease on large-scale brain networks. Physica D 454:133839

Škoch A, Rehák Bučková B, Mareš J, Tintěra J, Sanda P, Jajcay L, Horáček J, Španiel F, Hlinka J (2022) Human brain structural connectivity matrices-ready for modelling. Scientific Data 9(1):486

Stefanis L (2012) α-synuclein in Parkinson's disease. Cold Spring Harb Perspect Med 2(2):009399

Tolar M, Abushakra S, Sabbagh M (2020) The path forward in Alzheimer's disease therapeutics: reevaluating the amyloid cascade hypothesis. Alzheimer's & Dementia 16(11):1553–1560

Tora V, Torok J, Bertsch M, Raj A (2025) A network-level transport model of tau progression in the Alzheimer's brain. Mathematical Medicine and Biology A Journal of the IMA 42(2):212–238

Ullah R, Lee EJ (2023) Advances in amyloid-β clearance in the brain and periphery: implications for neurodegenerative diseases. Experimental Neurobiology 32(4):216

Ver Hoef JM (2012) Who invented the delta method? Am Stat 66(2):124–127

Wang W, Feng Z, Shu L, Hu Y, Chen Y, Zhang B, Huang H (2025) Bridging prion biology and alzheimer's disease: from pathogenic seeds to precision therapeutics. Front Mol Neurosci 18:1660151

Weickenmeier J, Jucker M, Goriely A, Kuhl E (2019) A physics-based model explains the prion-like features of neurodegeneration in Alzheimer's disease, Parkinson's disease, and amyotrophic lateral sclerosis. J Mech Phys Solids 124:264–281

Yuan K-H, Cheng Y, Patton J (2014) Information matrices and standard errors for mles of item parameters in irt. Psychometrika 79(2):232–254

Publisher's Note Springer Nature remains neutral with regard to jurisdictional claims in published maps and institutional affiliations.